Telomerase-independent survival leads to a mosaic of complex subtelomere rearrangements in Chlamydomonas reinhardtii

Frédéric Chaux, Nicolas Agier, Clotilde Garrido, Gilles Fischer, Stephan Eberhard, Zhou Xu

Telomerase-independent survival leads to a mosaic of complex subtelomere rearrangements in *Chlamydomonas reinhardtii*

Frédéric Chaux,[1,4] Nicolas Agier,[1,3] Clotilde Garrido,[1,3] Gilles Fischer,[1] Stephan Eberhard,[2] and Zhou Xu[1]

[1] *Sorbonne Université, CNRS, UMR7238, Institut de Biologie Paris-Seine, Laboratory of Computational and Quantitative Biology, 75005 Paris, France;* [2] *Sorbonne Université, CNRS, UMR7141, Institut de Biologie Physico-Chimique, Laboratory of Chloroplast Biology and Light-Sensing in Microalgae, 75005 Paris, France*

Telomeres and subtelomeres, the genomic regions located at chromosome extremities, are essential for genome stability in eukaryotes. In the absence of the canonical maintenance mechanism provided by telomerase, telomere shortening induces genome instability. The landscape of the ensuing genome rearrangements is not accessible by short-read sequencing. Here, we leverage Oxford Nanopore Technologies long-read sequencing to survey the extensive repertoire of genome rearrangements in telomerase mutants of the model green microalga *Chlamydomonas reinhardtii*. In telomerase-mutant strains grown for hundreds of generations, most chromosome extremities were capped by short telomere sequences that were either recruited de novo from other loci or maintained in a telomerase-independent manner. Other extremities did not end with telomeres but only with repeated subtelomeric sequences. The subtelomeric elements, including rDNA, were massively rearranged and involved in breakage–fusion–bridge cycles, translocations, recombinations, and chromosome circularization. These events were established progressively over time and displayed heterogeneity at the subpopulation level. New telomere-capped extremities composed of sequences originating from more internal genomic regions were associated with high DNA methylation, suggesting that de novo heterochromatin formation contributes to the restoration of chromosome end stability in *C. reinhardtii*. The diversity of alternative strategies present in the same organism to maintain chromosome integrity and the variety of rearrangements found in telomerase mutants are remarkable, and illustrate genome plasticity at short timescales.

[Supplemental material is available for this article.]

Protection of chromosome extremities is essential for genome integrity. For most eukaryotes, it is achieved by repeated DNA sequences called telomeres and by telomere-bound factors, which collectively prevent chromosome ends from being processed as DNA damage (Jain and Cooper 2010; de Lange 2018). Telomeres shorten with each round of replication owing to the end replication problem and are, in general, maintained by telomerase, a dedicated reverse transcriptase able to elongate telomeres de novo. In its absence, some telomeres eventually reach a critical length that triggers replicative senescence, an arrested state induced by the DNA damage checkpoint. Replicative senescence was shown in some species to increase genome instability owing to repair attempts and bypass of the checkpoint arrest through the adaptation to DNA damage process (Blasco et al. 1997; Lee et al. 1998; Chin et al. 1999; Artandi et al. 2000; Hackett et al. 2001; Hackett and Greider 2003; Maciejowski et al. 2015; Coutelier et al. 2018; Henninger and Teixeira 2020). In senescent cells that eventually escape cell cycle arrest, such as some precursor cancer cells, telomeres become dysfunctional and induce further genomic instabilities, a phenomenon termed telomere crisis (Artandi and Depinho 2009; Maciejowski and de Lange 2017).

The absence of telomerase therefore generates genome instabilities that stem from telomeres and take many shapes: point mutations, deletions/insertions, translocations, aneuploidy, duplications, and even more dramatic rearrangements, such as chromothripsis during telomere crisis (Maciejowski et al. 2015). The precise molecular mechanisms underlying these alterations are not all well understood but often involve classical and alternative nonhomologous end-joining (c- and a-NHEJ), homology-directed repair (HDR), including homologous recombination and break-induced replication (BIR), together with missegregation of chromosomes, breakage–fusion–bridge (BFB) cycles, and other dynamic phenomena that act in cascades over multiple cell divisions (McClintock 1941; Blasco et al. 1997; Hackett et al. 2001; Hackett and Greider 2003; Capper et al. 2007; Davoli et al. 2010; Jones et al. 2014; Maciejowski et al. 2015; Maciejowski and de Lange 2017).

Subtelomeres are the genomic regions adjacent to telomeres and often contain families of paralogous genes or pseudogenes, ribosomal DNA (rDNA) arrays, transposable elements, and other repeated sequences (Corcoran et al. 1988; Louis 1995; Kim et al. 1998; Fabre et al. 2005; Richard et al. 2013; Yue et al. 2017; Chaux-Jukic et al. 2021). Subtelomeres are often involved in telomere-associated rearrangements owing to their repetitive nature promoting HDR, replication fork stalling and template switching (FoSTeS), and BIR (Corcoran et al. 1988; Louis and Haber 1990; Linardopoulou et al. 2005; Kuo et al. 2006; Rudd et al. 2007;

[4]Present address: Laboratory for Marine and Atmospheric Biogeochemistry, Ruđer Bošković Institute, 10000 Zagreb, Croatia
[3]These authors contributed equally to this work.
Corresponding author: zhou.xu@sorbonne-universite.fr
Article published online before print. Article, supplemental material, and publication date are at https://www.genome.org/cgi/doi/10.1101/gr.278043.123. Freely available online through the *Genome Research* Open Access option.

Maestroni et al. 2017; Takikawa et al. 2017; Chen et al. 2018; Kim et al. 2019). Consistently, subtelomeres evolve rapidly even in closely related species and within species (Anderson et al. 2008; Yue et al. 2017; Otto et al. 2018; Kim et al. 2019; Young et al. 2020). In some species, in the absence of telomerase, telomeres can be stabilized using the alternative lengthening of telomeres (ALT) pathway, which depends on homologous recombination and uses repeated sequences found in telomeres and subtelomeres as substrates (Lundblad and Blackburn 1993; Nakamura et al. 1998; Zellinger et al. 2007; Cesare and Reddel 2010).

Genome alterations, especially structural variations (SVs), initiated by telomere shortening and dysfunction, despite being widely studied in different models including cancer cells, have been difficult to map exhaustively owing to the complex nature of the rearrangements and the frequent involvement of repeated sequences such as the ones found in subtelomeres (Maciejowski and de Lange 2017; Ho et al. 2020). Only recently were long-read sequencing technologies used to enable the resolution of complex rearrangements at chromosome extremities, in response to telomere shortening and dysfunction in *Caenorhabditis elegans* and *Saccharomyces cerevisiae* (Kim et al. 2021; Kockler et al. 2021; Sholes et al. 2021).

We recently provided a comprehensive map of all 34 subtelomeres of the unicellular green alga *Chlamydomonas reinhardtii* (17 chromosomes as haploid, 111 Mb) (Chaux-Jukic et al. 2021). All contain arrays of repeated elements, the most common being the *Sultan* element, present in 31 out of the 34 chromosome extremities in a haploid strain, arranged in tandem repeats of up to 46 elements (Supplemental Fig. S1A). The basic *Sultan* element has a length of ~850 bp and forms class A subtelomeres. The *Sultan* element of class B subtelomeres contains additional insertions. Next to most *Sultan* arrays (29 out of 31), a sequence of ~500 bp called *Spacer* is unique to each subtelomere and may serve as promoter for downstream noncoding RNA genes. The three remaining subtelomeres are entirely composed of rDNA, for a total of approximately 350 copies corresponding to ~3 Mb. Two other repeated elements, called *Suber* and *Subtile*, were found next to *Sultan* elements at three subtelomeres, called class C. The *Suber* element, initially named pTANC (Hails et al. 1993), contains the most abundant interstitial telomere sequence (ITS) of the genome. We previously found experimental evidence of telomere-associated genome rearrangements potentially involving subtelomeres in telomerase mutants of *C. reinhardtii*, correlated with long-term survival (Eberhard et al. 2019). Indeed, although some telomerase-negative mutant subclones underwent senescence-induced cell death, many managed to survive telomerase absence and must have therefore found a solution to maintain and protect telomeres. In this work, using long-read Oxford Nanopore Technologies ("Nanopore") sequencing able to traverse large repeated regions, we investigated genome instability in telomerase mutants in *C. reinhardtii* with the aim of providing an exhaustive view of the landscape of genome rearrangements. The rearranged genomic regions, most importantly telomeres and subtelomeres, were then scrutinized to provide insights into the mechanisms of chromosome-end plasticity and stability.

Results

Long-read Nanopore sequencing of prolonged cultures of telomerase mutants

To investigate the genome rearrangements induced by the long-term absence of telomerase, we used two different telomerase-mutant strains, *tel-m1* and *tel-m2* (Fig. 1A). The two mutant strains were obtained from the "*Chlamydomonas* Library Project" (CLiP) library of random insertion mutants (Li et al. 2016) and contained the paromomycin resistance gene inserted in the RNA-binding domain (*tert1-1* allele, corresponding to strain *tel-m1*) and catalytic domain (*tert1-2* allele, corresponding to strain *tel-m2*) of *TERT1* (also called *CrTERT*), the gene encoding the catalytic subunit of telomerase. For each mutant strain, the single insertion of the paromomycin resistance gene in *TERT1*, leading to an "ever-shorter telomere" phenotype, was confirmed previously (Eberhard et al. 2019). Upon receiving them from the Jonikas laboratory, we cultivated the mutant strains alongside the corresponding wild-type strain CC-4533 for an estimated 450 generations and collected the samples called "*tel-m1-1*," "*tel-m2-1*," and "WT CC-4533," respectively (Fig. 1A). As noted previously, we did not observe any obvious growth defect in these telomerase-mutant strains grown in standard culture conditions. For *tel-m1*, we also collected an earlier sample named "*tel-m1-0*," which corresponded to the earliest time point we could obtain upon reception of the strain in our laboratory. The strains had potentially experienced several additional prior passages, needed for the procedure of transformation, propagation, and freezing as described by Li et al. (2016).

We optimized a CTAB/phenol/chloroform purification protocol followed by a size-selection step to extract and obtain long DNA molecules (Chaux-Jukic et al. 2022). We then sequenced the genomic DNA of these four samples by long-read Nanopore sequencing and obtained four sets of high-quality reads of N50 > 14 kb and depth > 25× (Fig. 1A; Supplemental Table 1). We previously proved that long reads allowed the accurate reconstruction of the highly repeated subtelomere structures in *C. reinhardtii* (Chaux-Jukic et al. 2021), which is instrumental for the analysis of rearrangements potentially implicating telomeres, subtelomeres, and other repeated elements.

The long-read data sets were processed by three assemblers, allowing us to generate de novo genome assemblies of CC-4533 and each telomerase mutant (Fig. 1B,C; Supplemental Table 2). We reached large chromosome-scale scaffolds similar to the most contiguous reference genome of CC-1690 (Fig. 1B; O'Donnell et al. 2020). Sequencing depth (Fig. 1C, outer circles; Supplemental Fig. S1B) indicated a partial duplication of Chromosome 1 in CC-4533 not present in a previous sequencing (Gallaher et al. 2015), suggesting that a duplicated mini-Chromosome 1 emerged during the long-term culture in our laboratory, a phenomenon that is quite common because duplications were relatively frequent (although shorter) in mutation accumulation lines (López-Cortegano et al. 2023) and large duplications (up to ~400 kb) were observed in other laboratory wild-type strains (Flowers et al. 2015). The copy number variation (CNV) on Chromosomes 15 and 16 was because of frequently misassembled regions known to contain repeated sequences (Craig et al. 2023). No other chromosome-scale difference was found between CC-4533 and CC-1690 (Fig. 1B). The *Sultan* elements being present in 31 out of 34 subtelomeres and well assembled, we compared the number of *Sultan* elements at each chromosome extremity between CC-4533 and CC-1690 to evaluate their divergence at subtelomeres. We found that the number of *Sultans* for each extremity in these two strains was very close with few exceptions (Supplemental Fig. S1C). The subtelomeres of the wild-type CC-4533 strain have thus not been substantially altered during growth in this experiment and even since its selection as a laboratory strain decades ago, consistent with our previous finding that the subtelomeres have been very stable in laboratory strains (Chaux-Jukic et al. 2021).

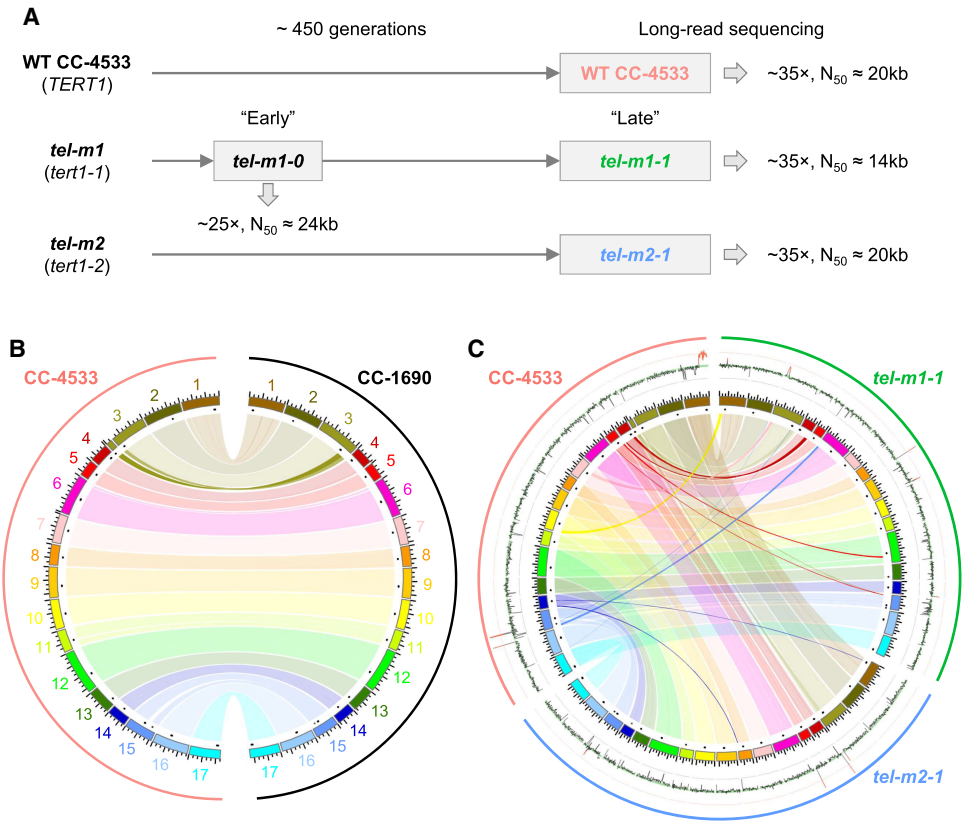

Figure 1. Independent genome assemblies of CC-4533 and telomerase-mutant strains *tel-m1-1* and *tel-m2-1* reveal few rearrangements at the genome assembly level. (*A*) Experimental setup and main sequencing output. (*B*,*C*) Circos plot (Krzywinski et al. 2009) of chromosome scaffolds from the long-term culture of CC-4533 compared with CC-1690 (*B*) and with *tel-m1-1* and *tel-m2-1* (*C*), shown as colored boxes, with black marks for centromere clusters (composed of the *Zepp-L1* repeat). Links connect homologous blocks, colored according to CC-4533 chromosomes. *Outer* plot displays sequencing depth, averaged over 100-kb regions, with 0×, 35×, and 70× grid lines shown in black, green, and red, respectively. Depth over 50× is highlighted in red, and genomic position is indicated in megabases.

Compared with CC-4533, *tel-m1-1* displayed a number of large-scale SVs and CNVs, corresponding to translocations and duplications of chromosome extremities (Fig. 1C; Supplemental Fig. S2A). The other mutant, *tel-m2-1*, showed fewer large-scale rearrangements in the assembly, but CNVs were detected at several locations, suggesting genome alterations (Supplemental Fig. S2B). We then used the SV caller MUM&Co (O'Donnell and Fischer 2020) to detect insertions, deletions, duplications, inversions, and translocations compared with CC-1690, and we found similar numbers for CC-4533 and the telomerase mutants assemblies, with about half of SVs shared by all three strains (n = 370 out of a total of 746) (Supplemental Fig. S2C,D). The assemblies of the telomerase mutants displayed a moderate number of unique SVs (n = 52 and 49 for *tel-m1-1* and *tel-m2-1*, respectively), involving sequences of median size < 600 bp.

However, we found that the quality of read mapping to subtelomeres was lower than that corresponding to the core genome both in CC-4533 and in the telomerase mutants (Supplemental Fig. S2E), presumably because the repeated elements found at subtelomeres present a challenge for genome assembly even using long-read sequencing data (Filloramo et al. 2021). Consistently, the assembled genomes reached only 25, two, and 19 telomeres in CC-4533, *tel-m1-1*, and *tel-m2-1*, respectively. We thus suspected that the assembly-level analysis would miss genome rearrangements affecting chromosome extremities. Additionally, assemblers were not designed to handle genome heterogeneity at the subpopulation level, which is likely to be the case in telomerase mutants. We therefore directly looked for genome alterations at the level of the sequencing reads instead of the assemblies in the rest of this work.

Telomere shortening and loss in telomerase mutants

We were first interested in investigating changes related to telomere sequences. To detect all telomere sequences at the level of individual reads, we developed a new method called TeloReader that scores 8-mers with respect to their level of identity to any of the canonical 8-mers (TTTTAGGG/CCCTAAAA and circular permutations) in sliding windows and uses thresholds for the average score to find the boundaries (see Methods). TeloReader allowed us to detect all telomere sequences of at least 16 bp, whether they were at a chromosome extremity (terminal) or not (interstitial, i.e., ITS), in the read data sets.

We measured the length of all terminal telomere sequences in the wild-type and mutant reads and found shorter telomeres in the mutants (mean ± SD for CC-4533: 293 ± 126 bp, *tel-m1-0*: 167 ± 109 bp, *tel-m1-1*: 162 ± 120 bp, *tel-m2-1*: 181 ± 88 bp) (Fig. 2A). Telomeres were already short in the *tel-m1-0* sample, and their length did not further decrease in the *tel-m1-1* sample, suggesting the stabilization of telomere length by telomerase-independent mechanisms or de novo telomere formation after complete loss.

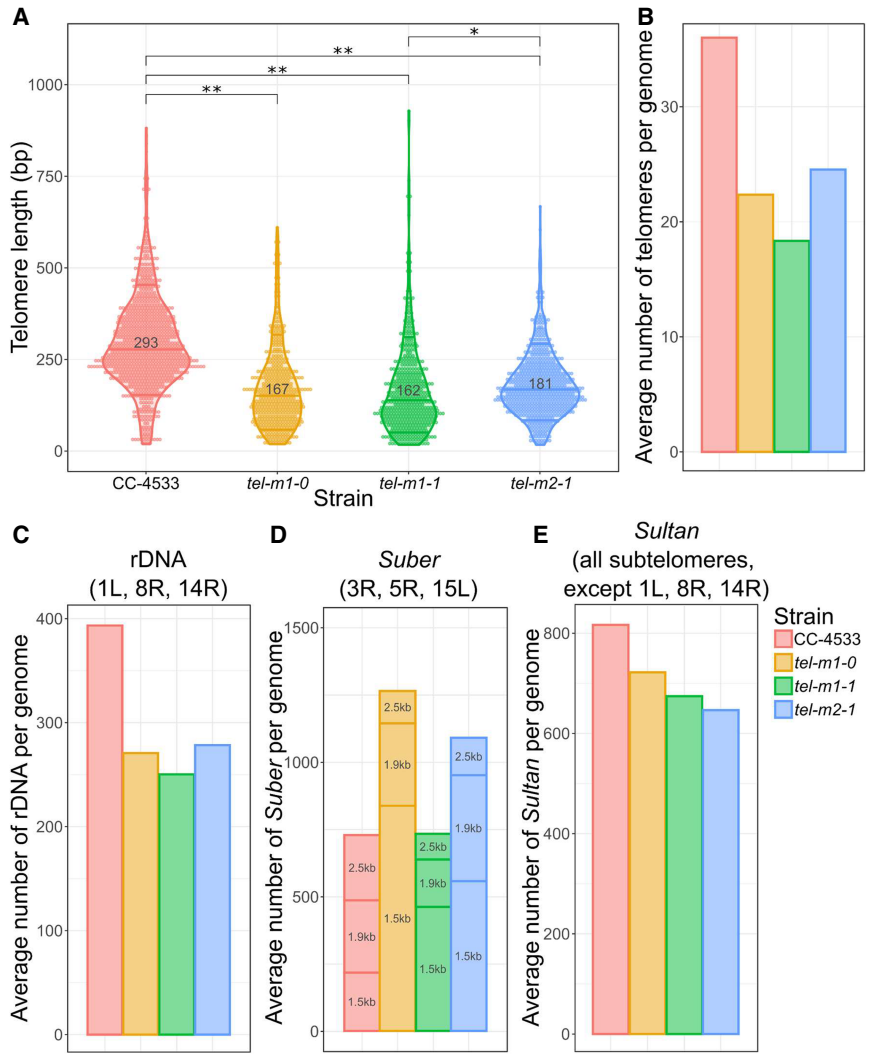

Figure 2. Telomere length distribution and CNVs of subtelomeric elements. (*A*) Telomere length distribution of terminal telomere sequences detected by TeloReader from the reads data set in CC-4533 and three telomerase mutant samples. Statistically significant difference: (*) *P*-value = 6.8×10^{-9} and (**) *P*-value < 2.2×10^{-16}, using a nonparametric Kruskal–Wallis test. (*B*) Number of telomeres in reads normalized by the sequencing depth. (*C–E*) CNVs for repeated elements normally found at subtelomeres including the rDNA (*C*), the *Suber* elements subdivided into three types according to their length ("1.5 kb," "1.9 kb," and "2.5 kb"; *D*), and the *Sultan* elements (*E*).

Extrachromosomal telomeric DNA molecules, predominantly found as double-stranded or single-stranded circles, are detected in ALT tumors and proposed to be involved in telomere maintenance (Cesare and Reddel 2010). To detect potential circular DNA containing telomere sequences, we performed rolling circle amplification (RCA) assays using the ϕ29 polymerase followed by qPCR to measure telomeric content compared with a control without ϕ29 amplification (Henson et al. 2017). As a positive control, we used a 4.4-kb yeast circular plasmid (pRS306), containing the *URA3* gene that we targeted for qPCR, which we spiked into CC-4533 genomic DNA at a relative concentration of 100 plasmid molecules per genome. Although RCA performed on the plasmid led to an approximately eightfold increase in *URA3* signal, no ϕ29 amplification of the telomeric content was detected for CC-4533 or the telomerase mutants (Supplemental Fig. S3B), suggesting that RCA templated by telomeric circles is likely not the main telomere maintenance mechanism in telomerase mutants in *C. reinhardtii*.

To test if a subset of telomere sequences was completely lost, we computed the total number of telomere-containing reads normalized to the sequencing depth of the nuclear genome and found that the average number of telomeres per cell was smaller in the mutants: 22 in *tel-m1-0*, 18 in *tel-m1-1*, and 25 in *tel-m2-1* versus 36 in CC-4533 (which has an extra mini-Chromosome 1 in addition to the 17 chromosomes) (Fig. 2B).

Overall, telomeres shortened as expected in telomerase mutants, but our data revealed the heterogeneity of shortening pattern at each specific telomere and suggested that telomeres were maintained or newly formed in *tel-m1-1* compared with *tel-m1-0* in a telomerase-independent manner. In the next sections, we investigate chromosomal rearrangements occurring at subtelomeric regions.

Because we suspected that the aggregate length distribution measurement would mask telomere length dynamics at each extremity, we assigned the reads containing a terminal telomere sequence to a specific chromosome arm based on the presence of specific and unique *Sultan* elements in the reads and measured telomere length distribution for each *Sultan*-associated extremity (Supplemental Fig. S3A). Out of the 27 studied class A and B extremities, eight showed telomeres further shortening between *tel-m1-0* and *tel-m1-1*, with large variations in the rate of shortening. They were stabilized or even slightly increased in length between *tel-m1-0* and *tel-m1-1* in 16 cases. In the remaining three extremities, the very low or even absence of reads in *tel-m1-0* and/or *tel-m1-1* prevented comparison and suggested the loss of the telomeric repeats or subtelomere sequence. Telomere length distribution at each extremity also displayed variations in *tel-m2-1*.

CNVs of subtelomeric elements in telomerase mutants

As a first insight into the stability of repeated subtelomeric elements (rDNA, *Suber*, and *Sultan*), we computed their CNVs in telomerase mutants compared with CC-4533.

We used the rDNA sequence as a query to find all reads containing rDNA. We observed an overall decrease of 31%, 36%, and 29% in rDNA copy number in *tel-m1-0*, *tel-m1-1*, and *tel-m2-1*, respectively, compared with CC-4533 (Fig. 2C). We also found that, although in the wild type, it was exclusively found at three subtelomeres as expected (Chaux-Jukic et al. 2021), rDNA could be mapped at several additional regions of the genome in telomerase

mutants, implicating rDNA in genome rearrangements (see below). The two major rDNA clusters at subtelomeres 8R and 14R likely lost a large fraction of their rDNA copies.

The same analysis was performed with the *Suber* element, which is found as three main subtypes of sizes ~1.5 kb, ~1.9 kb, and ~2.5 kb (Hails et al. 1993; Chaux-Jukic et al. 2021), and showed changes specific to each subtype (Fig. 2D). The copy number of the 1.5-kb element was greatly increased in the telomerase mutants compared with the wild type, especially in *tel-m1-0*, in contrast to the 2.5-kb element, which decreased in copy number in all mutants. The number of 1.9-kb elements only decreased in *tel-m1-1*. Given the organization of *Suber*s in arrays containing only one subtype (Chaux-Jukic et al. 2021), the different changes in copy number depending on the subtype likely reflected duplicated, deleted, and potentially rearranged arrays.

Finally, the *Sultan* element, the most abundant and widespread repeated element in subtelomeres, was decreased in copy number in both telomerase mutants (Fig. 2E).

Overall, all the main subtelomeric repeated elements showed CNVs in the telomerase mutants, indicating that subtelomeres are involved in chromosome rearrangements.

Contraction, erosion, and expansion of *Sultan* arrays

To analyze subtelomere structure, we looked for the presence of the *Spacer* element in all reads because this element is present as a single copy in 29 out of 34 subtelomeres in the wild-type strain, with sufficient sequence differences to uniquely identify the corresponding subtelomere (Chaux-Jukic et al. 2021). Reads containing a *Spacer* element were thus grouped according to their *Spacer* and displayed as a schematic representation of all the sequence features they contain (Supplemental Data Set 1).

Although for all *Spacers*, reads from CC-4533, even after hundreds of generations of culture, were consistent with a subtelomeric structure identical or nearly identical to the one we inferred from the genome assembly of CC-1690 (Supplemental Data Set 1; Supplemental Fig. S1C; Chaux-Jukic et al. 2021), reads from the telomerase mutants revealed many differences compared with CC-4533, including a large variety of rearrangements (Table 1; Supplemental Data Set 1).

We first focused on subtelomeres composed, in CC-4533, of an array of *Sultan* elements as the only repeated element, which are the vast majority (class A and B, 27 subtelomeres out of 34). In CC-4533, at each class A/B *Sultan* subtelomere, the reads were consistent with a single population of subtelomeres with a fixed number of *Sultans* and capped by telomeric repeats, as supported by a majority of reads (Fig. 3A,D). Reads that did not reach the extremity of the chromosome were explained by DNA molecules being physically broken during the extraction and preparation procedure and would be expected to terminate at random position in the *Sultan* array and within a *Sultan* element, which we confirmed (Fig. 3B,E). Additionally, in CC-4533, all reads containing simultaneously a specific *Sultan* element and a telomere sequence could be retrieved, and their number was often close to the number of *Spacer*-containing reads (Supplemental Fig. S4A), consistent with the fact that *Spacer*-containing reads did not always reach a telomere sequence because of the physical breakage of the extracted DNA molecule. Both telomerase mutants frequently showed reads that also supported a fixed number of *Sultans* (Fig. 3A,C). We call such subtelomeres "stabilized *Sultan* arrays." However, the number of *Sultan* elements could differ from CC-4533 (Fig. 3C): In *tel-m1-1* and *tel-m2-1* combined, we observed a decreased number of *Sultans* in six cases by two to 32 repeats, and in one case on the contrary, the number of *Sultan* elements was slightly increased by one. For the rest of the cases (n = 11), no variation of the number of *Sultans* was observed. We found that stabilized *Sultan* arrays in telomerase mutants were capped by short telomere sequences (Fig. 3A; Supplemental Figs. S3A, S4A), suggesting that these telomeres were maintained in a telomerase-independent manner.

We then asked whether at the extremities of stabilized *Sultan* arrays with a decreased number of *Sultan* elements (n = 6), the telomeres could be established de novo after complete loss or whether *Sultan* elements were excised internally independently of the initially present telomere sequence. To address this point, we identified the junction between the telomere sequence and the first *Sultan* element and compared it between CC-4533 and the

Table 1. Summary of rearrangements classified by types, found at *Spacer*-containing subtelomeres

	tel-m1-0	*tel-m1-1*	*tel-m2-1*
Similar to WT	9	7	9
Absence of *Spacer*	1	1	3
Contraction of *Sultan* array (stabilized)	3	1	5
Unstable *Sultan* array	3	3	4
Expansion of *Sultan* array (stabilized)	1	0	1
Fusion between *Sultan* arrays (total):	13	17	3
- Same orientation	3	5	1
- Inverted orientation	10	12	2
Recruitment of rDNA	4	5	1
Recruitment of other sequences	3	4	2
Breakage-Fusion-Bridge	4	5	0
Chromosome circularization	1	1	0
Heterogeneous subpopulations	7	9	4

The number of the described rearrangements/events found at *Spacer*-containing subtelomeres compared with CC-4533 is indicated. For subtelomeres with reads that represented multiple subpopulations ("heterogeneous subpopulations"), the rearrangements/events of each subpopulation were counted. Only rearrangements supported by at least two reads were taken into account.

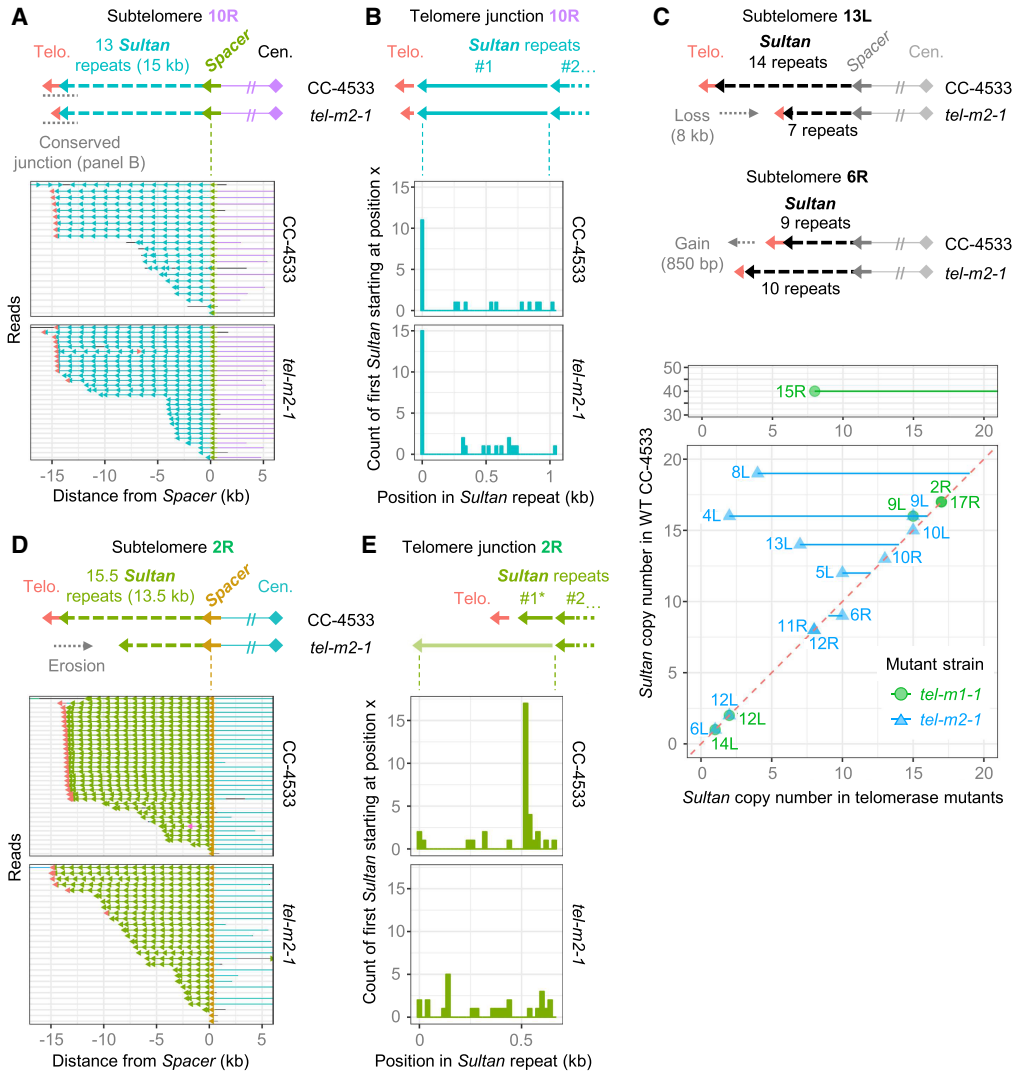

Figure 3. Contraction, erosion, and expansion of *Sultan* arrays. (*A*) The stabilized 10R *Sultan* array of *tel-m2-1* capped by a telomere sequence is depicted in comparison to CC-4533. Nanopore reads, colored based on the element (as indicated in the schematic representation; black segments correspond to sequences that did not align to any of the selected queries) and anchored at the *Spacer*, are shown. (*B*) For each read, the starting position of the *Sultan* element adjoining the telomere sequence is recorded, and the overall distribution of counts over the length of a *Sultan* element is represented. (*C*) Schematic representation of contraction and expansion of stabilized *Sultan* arrays (*top*) and overall changes in *Sultan* number in stabilized *Sultan* arrays for *tel-m1-1* and *tel-m2-1* (*bottom*). (*D*) Same as *A* with the unstable 2R *Sultan* array of *tel-m2-1*. (*E*) Same as *B* but for the unstable 2R *Sultan* array of *tel-m2-1*. (*) The first *Sultan* element in CC-4533 is partial.

mutants at the level of individual reads (Fig. 3B; Supplemental Fig. S4B). In two out of six shorter stabilized *Sultan* arrays (i.e., 4L and 5L in *tel-m2-1*), we found that the telomere sequence transitioned into the *Sultan* element at a different position within the *Sultan* compared with CC-4533, suggesting that the telomeres were added de novo on truncated *Sultans* (Supplemental Fig. S4A,B). In the remaining four cases (15R in *tel-m1-1* and 8L, 13L, and 9L in *tel-m2-1*), telomeres were found at the same position of the first *Sultan* in CC-4533 and the mutants, suggesting that changes in the number of *Sultan* elements of the array could also be because of excision of internal *Sultan* elements, without affecting the first *Sultan*.

At some subtelomeres (three for *tel-m1-1* and six for *tel-m2-1*), the reads were not consistent with a stabilized number of *Sultan* elements, and the vast majority had different counts, suggesting a heterogeneous population of cells in which that specific extremity shortened progressively. These *Sultan* arrays were qualified as "unstable." This situation is exemplified by subtelomere 2R in *tel-m2-1* (Fig. 3D). Consistent with a progressive erosion of the extremity, the first *Sultan* element ended at different positions of the *Sultan* element in different reads and was often not capped by telomere sequences (Fig. 3E; Supplemental Fig. S4A,B). To rule out that these reads containing a variable number of *Sultan* elements were not simply owing to physically broken DNA molecules, we searched for all reads containing simultaneously the same *Sultan* elements and telomeric repeats and compared their number with the number of reads containing the corresponding *Spacer* (Supplemental Fig. S4A). In contrast to CC-4533, unstable *Sultan* arrays in the mutants showed fewer telomere-containing reads than *Spacer*-containing ones, indicating telomere loss and supporting the idea that these extremities truly ended with *Sultan* elements. The progressive loss of telomeric repeats and *Sultan* elements was

consistent with the overall decrease in the number of telomeres and *Sultan* copy number (Fig. 2B,E). Erosion of *Sultan* arrays would eventually lead to their complete loss, a situation that we could clearly evidence for subtelomere 7L (Supplemental Fig. S5A): In *tel-m1-0*, the subtelomere contained only three *Sultans* compared with eight in CC-4533, but in *tel-m1-1*, the extremity was eroded beyond the *Spacer* and a new telomere was formed with the additional translocation, in a subpopulation of reads, of a sequence from Chromosome 11. The length distributions of the telomere sequence in these two subpopulations were consistent with their position as a terminal telomere sequence and ITS (Supplemental Fig. S5B). Analysis of the junctions revealed a 4-bp microhomology with the telomere sequence (Supplemental Fig. S5C). An analogous comparison between CC-4533, *tel-m1-0*, *tel-m1-1*, and *tel-m2-1* for the class C subtelomere 15L tended to suggest that *Suber* arrays could also be progressively eroded until completely lost (Supplemental Fig. S5D).

Finally, we asked whether there might be extrachromosomal circular *Sultan*-containing molecules preferentially enriched in telomerase mutants, which could act as templates to maintain *Sultan* subtelomeres or limit their erosion. We thus measured the *Sultan* content by qPCR in RCA products in CC-4533 and the telomerase mutants but found no ϕ29-dependent increase in any strain (Supplemental Fig. S3B).

Complex rearrangements within and between subtelomeres

In telomerase mutants, we observed a large fraction of telomere-containing reads with unusual combinations of subtelomeric elements (Table 1; Supplemental Data Set 1). To better characterize the structure of these rearranged subtelomeres, we again used the *Spacer*-based analysis to help anchor the reads to a given chromosome extremity.

Fusion between subtelomeric elements

Fusions of elements from different subtelomeres were the most frequent genome rearrangement occurring at subtelomeres (Table 1). The simplest type corresponded to the juxtaposition of two or more arrays of different *Sultan* elements, either in the same or in reverse orientations, such as subtelomere 6R in *tel-m1-0* (Fig. 4A) or subtelomere 15R in *tel-m2-1* (Supplemental Fig. S6A). Multiple subtelomeric elements of different types, such as rDNA and *Sultan* in subtelomere 6L of *tel-m1-0* and *tel-m1-1*, were also observed (Fig. 4B; Table 1). Because rDNA and *Sultan* do not share sequence homology, we speculate their fusion stemmed from NHEJ-dependent translocation events or end-to-end fusion.

The complexity of the observed genome rearrangements suggested that they formed through a multistep process. To test this hypothesis, we compared the rearrangements found in *tel-m1-0* to those in *tel-m1-1*, as these two samples were collected at different times. We could find intermediate rearrangement states in the earlier *tel-m1-0* sample, suggesting that at least some complex rearrangements were formed in multiple steps over time (Fig. 4B; Supplemental Figs. S5A, S6B). For example, at subtelomere 6L, the already complex structure found in *tel-m1-0* further changed in *tel-m1-1* and diverged into two structurally distinct subpopulations (Fig. 4B). As another example, subtelomere 17L displayed a reduced number of *Sultan* elements in *tel-m1-0* compared with the wild type with a subpopulation of reads capped by telomere sequences, representing a shortened stabilized *Sultan* array, but contained in *tel-m1-1* additional sequences from a $(CA)_n$ microsatellite, from Chromosome 15 and from 5R *Sultan* elements, and fused to the remaining 17L *Sultans* (Supplemental Fig. S6C).

Signature of BFB events

The read coverage mapped to the assembly of *tel-m1-1* genome identified a duplicated region at the extremity of Chromosome 9R (Fig. 4C, top). Closer inspection of the reads anchored by their *Spacer* element revealed a pattern of two inverted 9R *Sultan* arrays fused to each other in a head-to-head manner (Fig. 4C, middle). Each array was adjacent to its own 9R *Spacer* element and downstream 9R-specific sequences. Overall, this configuration was indicative of a fusion between sister chromatids followed by a breakage in anaphase, an event that initiated a canonical BFB cycle until the extremities were stabilized. We then looked for the new 9R extremity in *tel-m1-1* and identified the reads that mapped close to the 1×/2× coverage boundary. Reads that mapped only to the 2× side continued with at least two rDNA units over >11 kb (Fig. 4C, bottom). The rDNA sequence disrupted a RTEX-1 long interspersed nuclear element (LINE) retrotransposon framed by two arrays of MSAT-4B satellites, as shown in Figure 4C. What lay beyond the rDNA array remained unknown, in particular whether the extremity was capped by additional telomere sequences. In another example, the structure of the 11R extremity of *tel-m1-0* was consistent with at least two cycles of BFB, based on the multiple inverted repeats (Supplemental Fig. S6D). We found a total of five events consistent with BFB in *tel-m1-1* (Table 1), indicating that BFB cycles were a common mechanism at play once telomeres were lost.

Circularization of Chromosome 4

We report the head-to-head fusion of subtelomeres 4L and 4R in *tel-m1-1*, after complete loss of the telomere sequences and partial loss of *Sultan* elements (from 15 to two for 4L and from 21 to seven for 4R) (Fig. 4D). The de novo assembly of Chromosome 4 in *tel-m1-1* without relying on scaffolding with a reference sequence indicated that Chromosome 4 was made of a single contig with no extremity and had therefore a circular structure (Supplemental Fig. S6E,F). Circularization of the chromosome bypasses the need for functional telomeres to stabilize the extremities of linear chromosomes.

New telomeres outside canonical subtelomere regions lead to drastic chromosome rearrangements and karyotype alterations

We next investigated terminal telomere–containing reads not associated with the canonical subtelomeric elements, with the aim of revealing the formation of new extremities outside their normal subtelomeric contexts. Using TeloReader, we gathered all reads containing telomere sequences that were not associated to known subtelomeric elements (*Sultan*, *Spacer*, *Suber*, *Subtile*, or rDNA). We mapped these reads on the genome of CC-4533 and found such subtelomere-less telomeres at three and two locations in *tel-m1-1* and *tel-m2-1*, respectively. Consistent with the genome assembly, we also detected the new telomere-capped extremity of the duplicated mini-Chromosome 1 from CC-4533, which transitioned directly into the Chromosome 1 sequence through a microhomology and without a subtelomeric element or other exogenous sequence (Supplemental Fig. S1B).

At subtelomeres 14L in *tel-m2-1* and 7L in *tel-m1-1* (Fig. 5A; Supplemental Fig. S5A–C), the telomere sequences connected to the chromosome arm several kilobases away from the expected telomere location in CC-4533, and the corresponding arrays of *Sultan* repeats were lost, but without loss of annotated genes. At

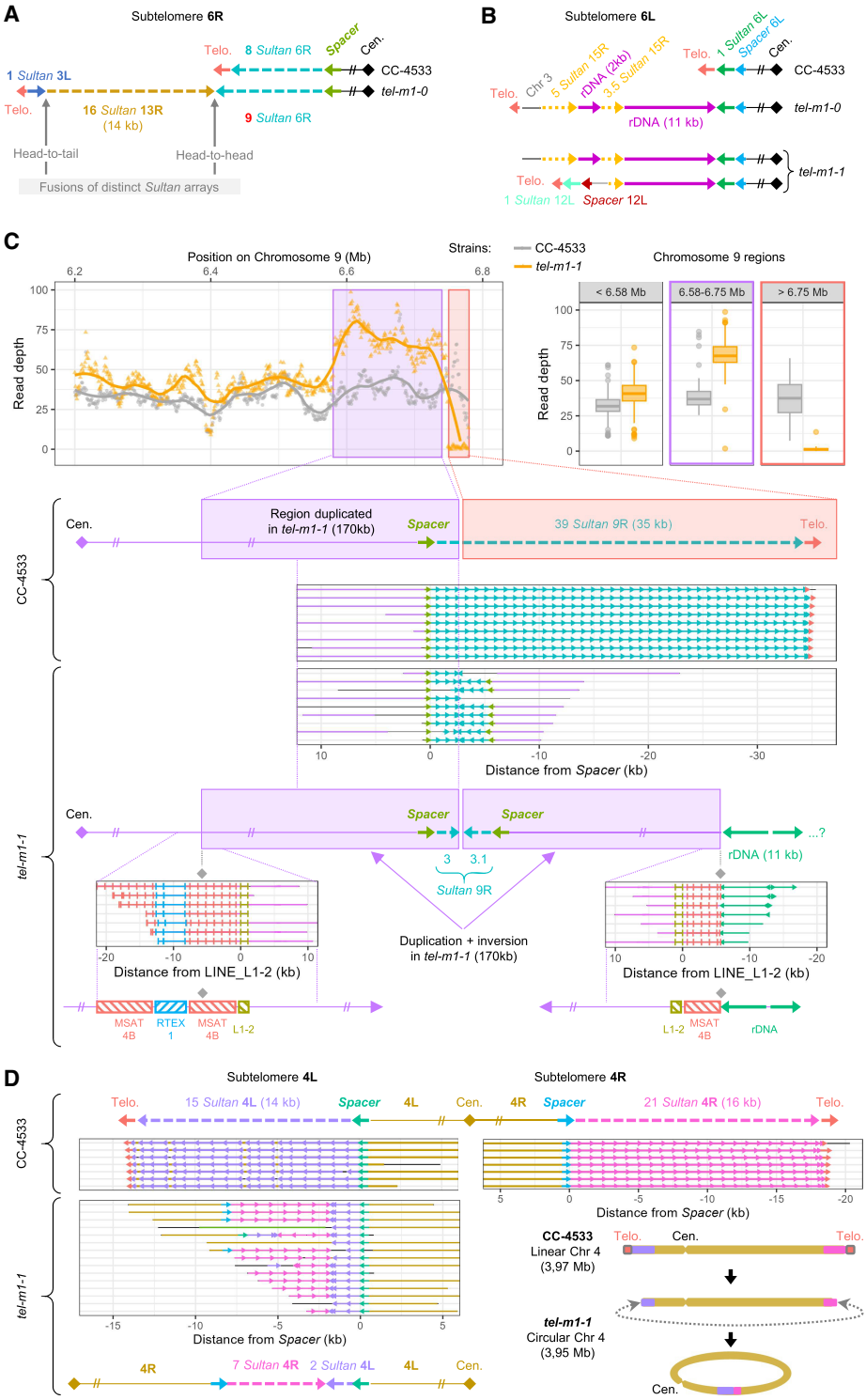

Figure 4. Complex genome rearrangements at subtelomeres. (*A*) Schematic representation of subtelomere 6R in which, in *tel-m1-0*, 2 additional *Sultan* arrays were fused to the initial *Sultan* array in inverted orientation. (*B*) Schematic representation of complex rearrangements at subtelomere 6L in *tel-m1-0* and *tel-m1-1*, including *Sultan* elements from different subtelomeres and rDNA sequences. In *tel-m1-1*, two subpopulations of reads reveal two distinct structures stemming from the initial rearrangement found in *tel-m1-0*. (*C*) Signature of a BFB event at subtelomere 9R in *tel-m1-1*. (*Top*) Duplication of the last 170 kb of the chromosome end. Read depth is computed on the indicated regions of Chromosome 9. (*Middle*) Individual reads supporting the loss of telomeres and 36 *Sultan* elements, as well as the end-to-end fusion of the 9R sister chromatids. (*Bottom*) Reads showing the recruitment of >11 kb of rDNA sequences at the new 9R extremity, disrupting an array of MSAT-4B satellite sequences. (*D*) Representation of reads supporting the fusion of subtelomeres 4L and 4R in *tel-m1-1*, after complete loss of telomeres and a total of 27 *Sultan* elements. (*Bottom right*) Scheme of the inferred circularization of Chromosome 4, also supported by de novo genome assembly (Supplemental Fig. S6E,F). Black segments correspond to sequences that are not aligned to any of the selected queries.

these novel telomere junctions, the chromosome arm showed no sequence homology with telomeric repeats, suggesting that the telomere was recruited at these sites by NHEJ rather than homology-mediated mechanisms.

The other new telomeres were involved in more complex rearrangements. The subtelomere 3L of *tel-m1-0* had 13 *Sultan* elements remaining after loss of the telomere sequence and four *Sultan* elements, followed by a short array of 13R *Sultan* elements and telomere sequence (Fig. 5B). Because it was present in a subpopulation of *tel-m1-0* reads and in *tel-m1-1*, this structure likely represented the first rearrangement step. Subtelomere 3L was further altered by the loss of the telomere and the fusion of 500 kb of duplicated sequence originally located at 2.1 Mb from the end of the left arm of Chromosome 7, which was then capped by a new telomere (Fig. 5B). Analysis of the junctions between these rearranged segments suggested that microhomology-dependent mechanisms were at play for the last step: junctions to telomeres (junction A) and to the 13R Sultan array (junction B) indeed involved microhomologies of 2–4 bp (Supplemental Fig. S7A,B). In contrast, the *Sultans* from 13R and 3L were connected with the insertion of a short sequence of unknown origin (junction C) (Supplemental Fig. S7C) but without homology or truncation of the neighboring *Sultan* elements, suggesting an NHEJ-dependent translocation that simultaneously incorporated a short piece of DNA.

On Chromosome 12 of *tel-m1-1*, the 2-Mb distal part of the right arm was translocated to the subtelomere 5L, and the new right end of Chromosome 12 carried a terminal telomere sequence preceded by a tandem duplication consisting of a fragment from Chromosome 12, nine telomeric repeats forming an interstitial array, and a short *Sultan* array from subtelomere 7L (Supplemental Fig. S7D,E).

In *tel-m2-1*, new telomeres were found at two close locations around the centromere of Chromosome 7, at the extremities of a 90-kb region displaying a 2× sequencing depth, indicating that the centromere was duplicated and the two arms of Chromosome 7 split into two telocentric chromosomes (Fig. 5C), thus constituting a Robertsonian fission, the reciprocal event of a Robertsonian fusion whereby two telocentric chromosomes are combined through their long arm with the loss of the very short arms and one centromere (Robertson 1916; Jones 1998). On the left end of the right arm, the new telomere capped an array of 7R *Sultan* lacking *Spacer* and a 65-bp ITS. On the right end of the left arm, the new telomere directly transitioned into the centromere.

Overall, duplications, nonreciprocal translocations, deletions, and more complex rearrangements created new extremities outside canonical regions and, in some cases, even altered the karyotype of the telomerase-mutant strains. For each new extremity, stability seemed to be ensured by newly recruited telomere sequences.

DNA methylation is maintained at chromosome extremities and at displaced *Sultan* arrays

We previously showed that *Sultan* arrays and, to a lesser degree, *Suber* arrays were hypermethylated, whereas the two major rDNA clusters were hypomethylated except for a few telomere-proximal repeats (Chaux-Jukic et al. 2021). *Sultan* subtelomeres are also associated with the heterochromatin mark H3K9me1 (Strenkert et al. 2013). Because subtelomeres in telomerase mutants were heavily rearranged, we asked whether DNA methylation remained associated with the *Sultan* elements that were no longer close to chromosome extremities and whether new extremities would acquire hypermethylation.

We thus base-called 5-methylcytosine (5mC) at CpG sites using Nanopolish (Simpson et al. 2017) and focused on rearranged loci. We first investigated the complex rearrangement found at extremity 3L of *tel-m1-1*, where a duplicated 500 kb of Chromosome 7 capped with telomeric repeats formed the new extremity and the original 3L *Sultan* elements were thus located much more internally (>500 kb) in the chromosome (Fig. 5B). To analyze 5mC content of the new extremity, we selected reads that aligned to the 500 kb of Chromosome 7 and at the same time contained the terminal telomere sequence and, in a second control group, reads that aligned to the 500-kb region but also continued beyond on Chromosome 7 (Fig. 6A; Supplemental Fig. S8A). The new 3L extremity was methylated over a length of ∼12 kb, whereas the same sequence on its original locus on Chromosome 7 was unmethylated and so was the same locus in the wild-type strain (Supplemental Fig. S8A). The 3L *Sultan* elements as well as the neighboring 13R *Sultans* in *tel-m1-1* maintained their high methylation status despite being now >500 kb away from the extremity (Fig. 6A).

That new extremities were hypermethylated even though they did not contain canonical subtelomeric sequences was confirmed at the truncated 14L extremity of *tel-m2-1* (Figs. 5A, 6B) and 7L of *tel-m1-1* (Supplemental Fig. S8B). Other examples of *Sultan* elements no longer located at subtelomeres but still methylated included the 4L and 4R *Sultan* elements of the circularized Chromosome 4 in *tel-m1-1* (Figs. 4D, 6C) and the head-to-head fused 9R *Sultan* elements, which resulted from the BFB event we described in a previous section (Figs. 4C, 6D). In the latter example, the *Sultan* elements were located at least 185 kb away from the new extremity. The reads mapping to the rDNA sequence at the 9R subtelomere showed that the rDNA was methylated (Fig. 6D), which in CC-1690 was only true for the rDNA of subtelomere 1L and a few telomere-proximal rDNA sequences at 8R and 14R subtelomeres, suggesting that the rDNA might constitute the new subtelomere of 9R in *tel-m1-1*. Subtelomere 16R in *tel-m2-1* provided another example of translocated rDNA, now directly between a terminal telomere sequence and Sultan elements, which was also hypermethylated (Supplemental Fig. S8C).

Overall, the *Sultan* elements that were no longer near chromosome extremities maintained their hypermethylation level. This observation was verified in all cases in *tel-m1-1* and *tel-m2-1* for *Sultan* arrays separated from the extremity by up to >500 kb of other nonmethylated sequences. Conversely, sequences that became capped by telomeres and formed new extremities acquired a hypermethylation pattern.

Discussion

Telomeres and subtelomeres are extensively implicated in genome instability induced by telomere shortening or dysfunction, as exemplified in post-telomere-crisis tumors (Maciejowski and de Lange 2017). Many types of telomere-related rearrangements have been studied in experimental systems of different model organisms and in tumor samples from patients. However, a direct assessment and comprehensive picture of the repertoire of genome rearrangements that functional telomeres protect from have rarely been achieved. Long-read sequencing has recently been used for genome assembly of *C. reinhardtii* and to assess the spectrum of SVs in various strains (Liu et al. 2019; O'Donnell et al. 2020; Craig et al. 2023; López-Cortegano et al. 2023; Payne et al. 2023). Here, we took advantage of long-read Nanopore sequencing to access telomere-induced SVs that would have escaped detection

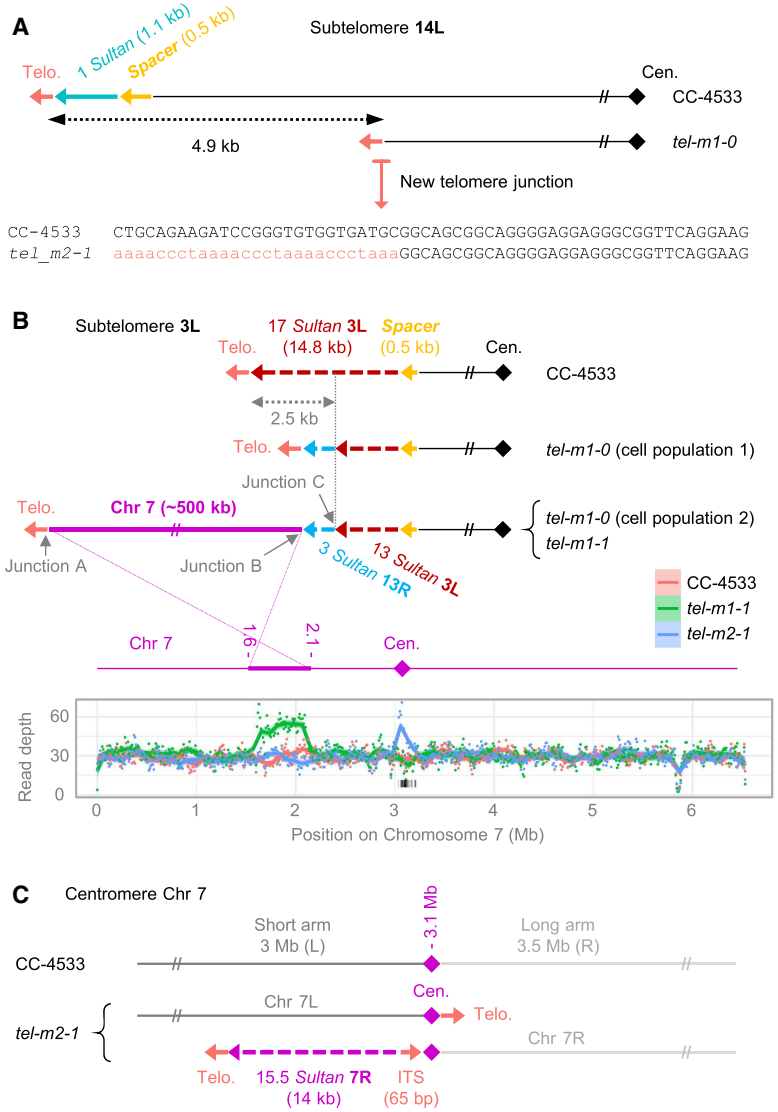

Figure 5. New extremities without canonical subtelomeric elements. (*A*) Scheme of the loss of 4.9 kb of sequence and formation of a new telomere at subtelomere 14L of *tel-m2-1*. The new junction sequence is shown. (*B*) Scheme of the complex new 3L extremity in *tel-m1-0* and *tel-m1-1*. The sequencing depth for Chromosome 7 is shown, revealing the duplicated 500-kb region in *tel-m1-1*. The sequences of Junction A, B, and C are shown in Supplemental Figure S7, A through C. (*C*) Scheme of the Robertsonian fission that occurred on Chromosome 7 of *tel-m2-1*. The new centromere-proximal extremities were stabilized by telomere sequences, with in addition a *Sultan* array and an ITS for the 7R long arm.

from short-read sequencing or at least would have been difficult to identify, particularly in repeated regions. We chose to sequence heterogeneous populations of telomerase-negative cells containing a complex mixture of subclonal genome rearrangements and to perform our analyses mainly at the level of reads, revealing mosaic rearrangement patterns that would have been missed in assembled genomes. A limitation of this approach is that we are unable in principle to assign specific rearrangements at different loci to the same cell or population of cells. However, most mosaic rearrangements we detected affect a substantial fraction of reads (typically > 10%–20%), and some are thus likely to co-occur in the same cell. On the other hand, rearrangements observed for all reads should be present in the vast majority of the population.

Alternative telomere maintenance

We previously showed that telomeres in *C. reinhardtii* are maintained by telomerase and that mutants of *TERT1*, the gene encoding its catalytic subunit, displayed an "ever-shorter telomere" phenotype, which led, in some telomerase-negative cultures derived from backcrosses, to growth defect and cell death consistent with senescence (Eberhard et al. 2019). Because they appear to maintain their telomeres at a short equilibrium length and do not display obvious growth defects, the *tel-m1* and *tel-m2* mutants are possibly already in a postsenescence state, although this remains to be shown formally. In this work, analysis of chromosome extremities in the long-term cultures of telomerase mutants showed that overall ~60% were still capped by short telomere sequences, reminiscent of type I postsenescent survivors in *S. cerevisiae* (Lundblad and Blackburn 1993; Teng and Zakian 1999). For at least a subset of them, the telomere sequence was likely recruited de novo on a truncated subtelomere or on a new chromosome extremity without canonical subtelomere by nonreciprocal translocation, as shown before for cancer cell lines (Sabatier et al. 2005). In all cases, telomeres were maintained, albeit at a short length distribution, which implied that an alternative maintenance mechanism was used, relying, for example, on homologous recombination or BIR but most likely without using extrachromosomal telomere circles.

A number of chromosome extremities completely lacked telomere sequences, and their lost telomeres might have been translocated to the new telomere sites we described. Individual read analysis of such telomere-less extremities showed that the *Sultan* array composing the subtelomere displayed a length distribution at the population level consistent with progressive loss of sequence. This observation leads to the intriguing possibility that the array of *Sultan* elements might directly function in end protection instead of telomeric repeats. Consistently, in end-to-end fusion events involving *Sultan* arrays (e.g., Fig. 4C,D), fewer than 10 *Sultan* elements were left when fusion occurred, which might suggest that larger *Sultan* arrays could confer some partial telomere protection. The *Sultan* element must then ensure telomere protection by, for example, binding a yet-unknown factor, which might be achieved through the short telomere-like sequence at the beginning of the element (Chaux-Jukic et al. 2021) or through another intrinsic binding site. Because *Sultan* elements are associated with heterochromatin, indirect binding of factors on modified histones might also provide sufficient protection, as proposed for *Drosophila melanogaster* and

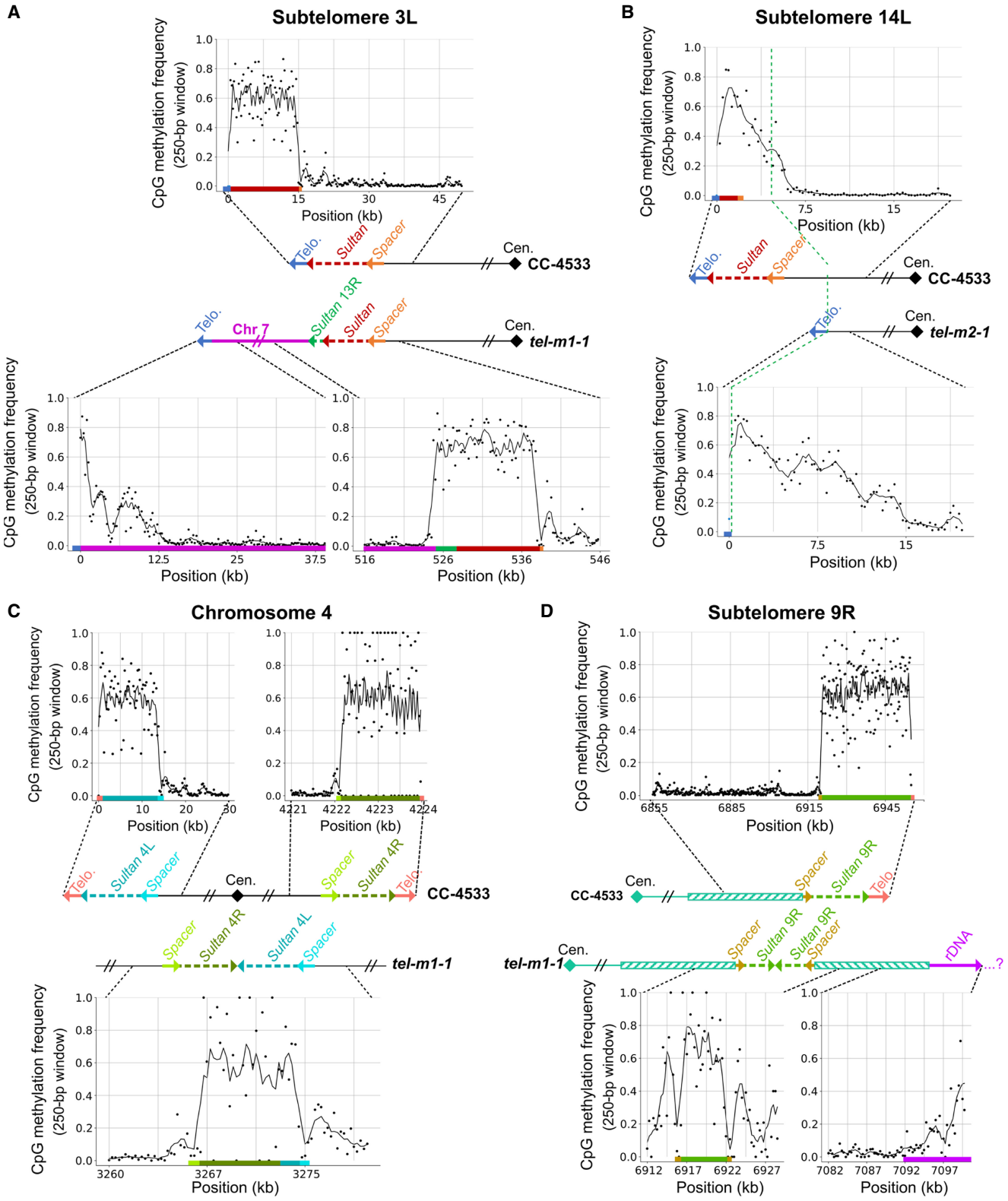

Figure 6. Methylation frequency of new extremities and displaced *Sultan* elements. (*A–D*) Analysis of 5mC frequency at CpG sites using reads that unambiguously spanned the indicated regions, in different illustrative cases. (*A*) At the rearranged 3L chromosome arm of *tel-m1-1*. Methylation frequency was plotted over different regions of subtelomere 3L in *tel-m1-1* and in CC-4533 as depicted. For the methylation frequency at Chromosome 7 in CC-4533 and *tel-m1-1*, see also Supplemental Figure S8A. (*B*) At the broken 14L subtelomere of *tel-m2-1*, where the internal genomic sequence was then capped by a telomere sequence, compared with CC-4533. (*C*) At the fused 4L and 4R *Sultan* arrays of *tel-m1-1*, compared with the two arrays in CC-4533. (*D*) At the head-to-head fused 9R *Sultan* arrays and the transition to rDNA in *tel-m1-1*, compared with the 9R extremity of CC-4533.

some telomerase-negative *Schizosaccharomyces pombe* survivors (Gao et al. 2010; Jain et al. 2010). Consistently, even when the chromosome extremities are not composed of *Sultan* elements, but of rDNA repeats or even other sequences, the DNA sequence is highly methylated (see discussion below).

Another strategy to maintain chromosome integrity without telomerase consists in chromosome circularization, which we observed for Chromosome 4 in *tel-m1-1*. Although we encountered only one such circularization event, the fact that we did not detect another subpopulation with another structure for Chromosome 4 suggests that this circular chromosome conferred some selective advantage (e.g., telomerase-independent genome integrity) or at least was not counter-selected. A similar circularization strategy in response to telomerase absence or disruption of telomere protection was also described in other eukaryotes (Naito et al. 1998; Nakamura et al. 1998; McEachern et al. 2000; Wu et al. 2020; Baumann and Cech 2001) and therefore appears to be relatively well tolerated across evolution.

Overall, although they came at the cost of wide-spread genome rearrangements, the diversity of alternative strategies to maintain chromosome integrity in telomerase mutants found in a single organism is remarkable and illustrates genome plasticity at short timescales.

Mechanisms of genome rearrangements in telomerase mutants

Because the approach used in this work consists in a direct visualization of chromosome sequences on a large scale with as little source of bias as possible, we were able to document a large variety of rearrangements. The fact that most rearrangements involved telomeres and subtelomeres suggested that critically short or dysfunctional telomeres preferentially induced local instabilities, which can propagate through various mechanisms such as BFB cycles involving dicentrics, as reported in yeast and human tumors (Hackett et al. 2001; Hackett and Greider 2003; Pobiega and Marcand 2010; Beyer and Weinert 2016; Maciejowski and de Lange 2017; Umbreit et al. 2020).

Short or dysfunctional telomeres, at the senescence stage or during crisis, can lead to end-to-end fusions as observed across evolution (Chan and Blackburn 2003; Mieczkowski et al. 2003; Heacock et al. 2004; Pardo and Marcand 2005; Capper et al. 2007; Lowden et al. 2008), although telomere sequences themselves may be completely absent at fusion sites in telomerase-negative cells (Blasco et al. 1997; Naito et al. 1998; Nakamura et al. 1998; Hackett et al. 2001). Despite many instances of end-to-end fusions, we found no remaining telomere sequences at fusion sites in our read data sets, suggesting that in *C. reinhardtii*, even very short telomeres might be sufficient to inhibit fusions. Instead, we detected many subtelomere–subtelomere fusions, the most frequent involving *Sultan* arrays. They can occur between different subtelomeres, as in the case of Chromosome 4 circularization, or between sister chromatid subtelomeres. Sister chromatid fusions were followed by cycles of BFB, propagating genome instability over multiple divisions and over more internal genomic regions, as for extremity 9R in *tel-m1-1*. Of note, we did not find any signature of chromothripsis resulting from the aberrant repair of the fragmentation of a chromosomal region, despite chromothripsis being associated with BFB cycles and telomere crisis in cancer (Garsed et al. 2014; Li et al. 2014).

Most rearrangements implicated the repeated elements that are found at the subtelomeres, which could promote homology-mediated mechanisms for amplification, deletion, and translocation. The activation of these mechanisms could contribute to the alternative maintenance strategy, but these rearrangements could also have been induced during senescence and crisis before the emergence of postsenescence survivors. We note, however, that if we assume that *tel-m1-0* already represented a postsenescent state, rearrangements were still ongoing between *tel-m1-0* and *tel-m1-1*, thus suggesting that they were not limited to the senescence stage. When different types of elements were found juxtaposed, the transition sequence often involved microhomologies of a few base pairs (e.g., Fig. 5B; Supplemental Fig. S7A,B), suggesting that mechanisms such as microhomology-mediated break-induced replication (MMBIR) (Payen et al. 2008; Hastings et al. 2009) or microhomology-mediated end-joining (MMEJ) (Sfeir and Symington 2015) might be involved. Even when no homology or microhomology was detected at junctions, canonical subtelomeric elements were still frequently found in rearrangements. We speculate that these subtelomeric elements were frequently excised from their native locus owing to terminal instability and were therefore available in subsequent fusion events. Nevertheless, other internal genomic regions were sometimes duplicated and translocated to chromosome ends, supporting the idea of a genome-wide increase in genome instability in telomerase-negative cells (Blasco et al. 1997; Lee et al. 1998; Chin et al. 1999; Hackett et al. 2001; Coutelier et al. 2018).

New chromosome extremities establish heterochromatin

We found new chromosome extremities that were capped by telomere sequences, suggesting that, in *C. reinhardtii*, telomeric repeats by themselves are sufficient for end protection in a context devoid of canonical subtelomeric elements. These new telomere-capped chromosome extremities formed by sequences originating from internal genomic regions showed high levels of 5mC. We therefore speculate that telomeres can establish new DNA methylation domains in *C. reinhardtii*, likely to be associated with heterochromatin. Although the heterochromatic nature of telomeres and subtelomeres is conserved in eukaryotes (except for *Arabidopsis thaliana* where it is less well established) (Gottschling et al. 1990; Baur et al. 2001; Koering et al. 2002; Pedram et al. 2006; Vrbsky et al. 2010; Vaquero-Sedas et al. 2011; Elgin and Reuter 2013; Matsuda et al. 2015), whether and how heterochromatin forms at a new telomere are less well known across organisms. The detection of new extremities in our work thus provides an additional piece of evidence for heterochromatin formation spreading from the telomere sequence being a property of chromosome extremities. Because many chromosome extremities were not capped by telomere sequences but directly by the hypermethylated *Sultan* arrays, one can speculate that heterochromatin might be a functional feature of a protected extremity in telomerase mutants of *C. reinhardtii*.

We note that *Sultan* elements that are displaced from their normal subtelomeric location retain a high level of 5mC, even when found at >500 kb of the extremity of the chromosome. Because we previously showed that *Sultan* elements are exclusively found at subtelomeres in wild-type strains, we propose that their sequence coevolved with their function at subtelomeres, so that they might recruit methyltransferases to actively contribute to heterochromatin maintenance and spread. This property would allow them to remain hypermethylated even when displaced from subtelomeres. In most cases, the *Spacer* sequence still acted as the boundary of the hypermethylated domain even when not located at subtelomeres.

To conclude, our results show that *C. reinhardtii* telomerase-negative cells use a variety of strategies to protect chromosome extremities, including the establishment of DNA methylation, and undergo diverse and complex rearrangements, highlighting a remarkable plasticity of the genome. This work shows the potential of long-read sequencing to provide a comprehensive view of complex genome rearrangements even in mosaic populations of cells at the level of subclones, an analysis that could be applied to tumor genome heterogeneity.

Methods

Strains and growth conditions

Wild-type CC-4533 and *tel-m1* (CLiP library identifier: LMJ.RY0402.077111; *tert1-1* allele) and *tel-m2* (CLiP library identifier: LMJ.RY0402.209904; *tert1-2* allele) mutant strains were obtained from the Jonikas laboratory (Li et al. 2016). They were maintained on plates in TAP medium (Harris 2009) at 25°C under low light (5 µE/m^2/sec) and restreaked in bulk without subcloning. Before DNA extraction, cells were grown in 200 mL liquid TAP medium until they reached ~2×10^7 cell/mL and collected by centrifugation at 5000*g* for 5 min. We previously confirmed for each mutant strain that the single insertion of the paromomycin resistance gene in *TERT1* (gene identifier: Cre04.g213652_4532) disrupted the RNA-binding domain (*tert1-1*) or the catalytic domain (*tert1-2*), both essential for telomerase function (Eberhard et al. 2019). This was performed by PCR with primers flanking the gene, in the gene, and/or in the paromomycin resistance gene, followed by sequencing of the PCR products. The single insertion was verified by backcrossing to a wild-type strain and, after meiosis and tetrad dissection, the 2:2 segregation of the insertion, of the resistance phenotype, and of the short telomere phenotype. The single insertion was also confirmed in the genome assemblies of the mutants.

DNA extraction and size selection

To extract genomic DNA while preserving high-molecular-weight fragments, we developed a modified version of a Joint Genome Institute protocol (https://www.pacb.com/wp-content/uploads/2015/09/DNA-extraction-chlamy-CTAB-JGI.pdf), as described by Chaux-Jukic et al. (2022). The extraction is followed by a clean-up using magnetic beads and size selection based on solid-phase reversible immobilization (Stortchevoi et al. 2020) using the SRE kit (Circulomics).

RCA assay

RCA followed by qPCR detection and analysis was performed as described previously (Henson et al. 2017), with minor adaptations. Briefly, for each sample, 80 ng of genomic DNA in 10 µL of Tris (pH 7.6) was mixed with 10 µL of the ϕ29 reaction buffer with or without 7.5 units of ϕ29 (Thermo Fisher Scientific). The reaction was then performed for 10 h at 30°C , followed by ϕ29 inactivation for 20 min at 70°C. As a positive control, 0.32 ng of the yeast plasmid pRS306 containing the *URA3* gene was spiked into 80 ng of CC-4533 genomic DNA, representing 100 plasmid molecules per genome. For detection of the reaction product, each sample was diluted fourfold, and 4 µL was used in a 20-µL qPCR reaction with Fast SYBR Green (Applied Biosystems) following the manufacturer's instructions and run in a CFX96 real-time PCR detection system (Bio-Rad). Technical qPCR triplicates were performed for each sample. We designed the following qPCR primers: for *URA3*, 5′-ATGTCGAA AGCTACATATAAGG-3′ (oZX180) and 5′-TAGTAAACAAATTTTGG GACCT-3′ (oZX568); for telomere sequences, 5′-GGTATTTGTCAG GGTGTTAGGGTGTTAGGGTGTTAGGGT-3′ (oZX576) and 5′-TCC CGACTATATCCCGAAAACTCTAAATCCCTATAACCCTA-3′ (oZX578); for the *Sultan* element, 5′-GGCTGCGTGGCTGGACTGCTGCA CT-3′ (oZX579) and 5′-CATTTCTGACATGTCACACTTTTCAAA-3′ (oZX572); and for *ATPC*, 5′-TCGTTCATTGCTCAGGAGTC-3′ (oZ X574) and 5′-AGCTTGAAGATCTCGTCGTC-3′ (oZX575). *ATPC* is a single-copy nuclear gene, which we used for normalization. To design the primers for telomere detection, we adapted a strategy previously developed (Cawthon 2002) for the human telomere motif to *C. reinhardtii*'s: We added 6 nucleotides not matching the telomere sequence at the 5′ end of each primer, and we introduced several additional mismatches that do not impede annealing to the telomere sequence and PCR but prevent primer dimerization.

Library preparation and sequencing

Sequencing libraries were prepared from SRE-treated high-molecular-weight DNA (except for *tel-m1-1*, which was sequenced in two runs, one without SRE treatment and one with), following Oxford Nanopore Technologies (ONT) protocols for genomic DNA without preamplification. Kits LSK109 and LSK110 were obtained from ONT and companion module NEBNext from New England Biolabs (NEB). As a minor modification, we started the preparation with 3 µg of DNA. The second *tel-m1-1* library was barcoded using barcode NB07 from kit NBD104 (ONT).

DNA libraries were sequenced on R9.4 or R10.4 Nanopore flow cells in a MinION Mk1C sequencer with default parameters on the MinKNOW operating software, except for the base-calling with Guppy, which was set to real-time high accuracy, and for the MUX scan, which was decreased to 1 h. For each run, 500 ng of DNA was loaded and sequenced for 8–12 h. The flow cell was then washed using the wash kit (ONT) and reloaded with the same sample, up to four times.

Genome assembly

Reads in FASTQ files and with quality > 7 were processed using Porechop with default parameters (https://github.com/rrwick/Porechop), for removing adapters/barcodes and splitting artifactual chimeras. Reads were assembled using Canu (Koren et al. 2017), SMARTdenovo (Liu et al. 2021), and NextDenovo (https://github.com/Nextomics/NextDenovo) using default parameters, and all chromosomes were successfully represented by one main contig. These draft assemblies were polished using Racon (Vaser et al. 2017; https://github.com/lbcb-sci/racon) and Medaka (ONT; https://github.com/nanoporetech/medaka) with the same reads and then scaffolded on the CC-1690 reference genome using RagTag (Alonge et al. 2022; https://github.com/malonge/RagTag). These assemblies were compared with each other and with references (CC-1690, CC-4532) using D-genies (Cabanettes and Klopp 2018; https://github.com/genotoul-bioinfo/dgenies) to assess contiguity. To generate a genome model for each strain, we chose for each chromosome the assembly giving the most colinear chromosome with CC-1690.

To test if Chromosome 4 of *tel-m1-1* was circular at the assembly level without relying on a reference genome for scaffolding, we used the assembler Flye (Kolmogorov et al. 2019; https://github.com/fenderglass/Flye), as it generated contigs long enough for this purpose. Visualization of the circular Chromosome 4 was performed using Bandage (Wick et al. 2015; https://rrwick.github.io/Bandage/).

Telomere sequence detection

To detect telomere sequences in individual Nanopore reads, we developed TeloReader, a Python (v3.9.12) script with only three dependencies (pandas [v1.4.3], numpy [v1.19.5], and Matplotlib [v3.5.1]). TeloReader scans each read in both directions, from 5′ to 3′ and from 3′ to 5′, to search for the C-rich telomere motif and the G-rich one, respectively. In the first step of TeloReader, the DNA sequence is transformed into a series of scores corresponding to the best alignment score (using pairwise2 from the package Biopython [v1.79]) of each 8-mer against all eight circular permutations of the telomere motif (CCCTAAAA for the C-rich and TTTTAGGG for the G-rich). This score is between zero and eight, but all scores lower than four are replaced by four to reduce the impact of sequencing errors in the following step. The second step defines the sequence in a sliding window of 15 bp (size_window) as telomeric if the average score is greater or equal to seven (min_mean_window). In a third step, consecutive overlapping telomeric sliding windows are merged to form a single telomere sequence. We added other constraints and rules to ensure the specificity and sensitivity of TeloReader: The minimal length of a telomere sequence is set at 16 bp (min_len); a telomere sequence must contain at least eight scores of eight; and a configuration in which a nontelomeric sequence is found between two telomere sequences (as defined after the third step) can be considered as a telomere sequence if the nontelomeric sequence is <20 bp (max_size_gap) and if the average score of the whole sequence encompassing the two telomere sequences and the nontelomeric sequence in-between is greater than 6.5 (min_mean_telo). A telomere sequence is considered as terminal if it is found at <50 bp from the extremities of the input sequence (3′ extremity for a C-rich telomere and 5′ extremity for a G-rich telomere). See Data access section below.

5mC detection

To detect 5mC in a CpG context, we used nanopolish (Simpson et al. 2017; https://github.com/jts/nanopolish) on the FAST5 files and their associated FASTQ files. Reads were aligned to their corresponding genome assembly using minimap2 (Li 2018; https://github.com/lh3/minimap2). Alternatively, for detection of 5mC in subpopulations, reads were first selected using fast5_subset (https://github.com/nanoporetech/ont_fast5_api) and aligned to a consensus sequence obtained through a multiple alignment using ClustalW (Larkin et al. 2007). The frequency of methylation for each base was obtained using nanopolish call-methylation and the script calculate_methylation_frequency.py.

Bioinformatic analysis

For genome-to-genome comparison, genome models were aligned against references genomes (CC-1690 and CC-4533) using minimap2 (Li 2018) and visualized with Circos plots (Krzywinski et al. 2009). The SV caller MUM&Co (O'Donnell and Fischer 2020; https://github.com/SAMtoBAM/MUMandCo) was used for structural variant detection and classification. For read analysis, reads were mapped to genomes using minimap2 with the following parameters: -a -x map-ont -K 5M -t 3. We used Integrative Genome Viewer (IGV) (Robinson et al. 2017; https://igv.org/) and Tablet (Milne et al. 2013; https://ics.hutton.ac.uk/tablet/) to visualize read mapping. To calculate sequencing depth, the genomes were divided into windows using "makewindows" from BEDTools (Quinlan and Hall 2010; https://bedtools.readthedocs.io/en/latest/index.html), and then depth was averaged over the windows using "bedcov" from SAMtools (Li et al. 2009; https://www.htslib.org/) with the following parameters: -g SUPPLEMENTARY with or without -q 60.

For read-level analysis, subtelomeric elements (*Spacer*, *Sultan*, rDNA, and *Suber*) were searched in reads using BLASTN (Altschul et al. 1990) with the following parameters: -max_target_seqs 10000 -evalue 0.001 -outfmt "6 qaccver qlen saccver slen pident length mismatch gapopen qstart qend sstart send evalue bitscore." Multiple hits at close positions were filtered using a custom bash script: Hits were sorted by decreasing order of bitscore (*sort* -rgk 14), and overlapping matches were eliminated. Reads containing subtelomeric elements or telomere sequences (detected by TeloReader) were further blasted against a library of repeated elements (Craig et al. 2021) and against reference genome, both of which were then filtered as above to exclude multiple matches. Annotations from all BLAST hits were then plotted on reads using R statistical software (R Core Team 2021). All lists of filtered BLAST hits lists were merged with "bind_rows"; reads of interest were identified (e.g., match to a given *Spacer* or *Sultan*) with "filter"; and all hits on this read subset were extracted with "semi_join." To order these reads, first, an anchor was selected, most often a specific *Spacer* sequence, allowing setting an origin and the orientation of each read. From these two pieces of information, new coordinates were recalculated for each hit along the reads and for read extremities. Hits were then plotted with distinct reads along the *y*-axis and coordinates along the *x*-axis (e.g., Figs. 3A,D, 4C, D). Because of the error rate of Nanopore sequencing at the raw read level together with rare artifactual chimeric reads (Delahaye and Nicolas 2021), we only describe rearrangements structurally supported by at least two reads.

Computations were mostly run on the cluster of the French Institute of Bioinformatics (https://www.france-bioinformatique.fr/en/home/).

Data access

All sequencing data, which include raw Nanopore FAST5 files and read FASTQ files, and genome assemblies (as FASTA files) generated in this study have been submitted to the European Nucleotide Archive (ENA; https://www.ebi.ac.uk/ena/browser/home) under project accession number PRJEB59713. The code for TeloReader is available as Supplemental Code and at GitHub (https://github.com/Telomere-Genome-Stability/Telomere_2023/tree/main/TELOREADER).

Competing interest statement

The authors declare no competing interests.

Acknowledgments

We thank Olivier Vallon for his critical reading of the manuscript, Maria Teresa Teixeira for reagents and plasmids, and Oana Ilioaia for her technical assistance. Research in G.F.'s laboratory was supported by the French National Research Agency ("ANR" grants ANR-16-CE 12-0019 and ANR-18-CE12-0004). Research in Z.X.'s laboratory was supported by ANR grant "AlgaTelo" (ANR-17-CE20-0002-01), by Ville de Paris (Programme Émergence[s]), and by the French National Cancer Institute (grant INCa_15192). S.E. was supported by the "Initiative d'Excellence" program of the French State ("DYNAMO," ANR-11-LABX-0011-01). F.C. is currently supported by a Marie Skłodowska-Curie Actions Postdoctoral Fellowship (101064365 Cocco-Next).

Author contributions: Investigation was by F.C., N.A., C.G., and S.E. Conceptualization was by F.C., G.F., S.E., and Z.X.

Methodology was by F.C., N.A., and C.G. Software was by F.C. and C.G. Formal analysis was by F.C., N.A., C.G., and S.E. Supervision was by G.F. and Z.X. Writing of the original draft was by F.C. and Z.X. Reviewing and editing were by all authors.

References

Alonge M, Lebeigle L, Kirsche M, Jenike K, Ou S, Aganezov S, Wang X, Lippman ZB, Schatz MC, Soyk S. 2022. Automated assembly scaffolding using RagTag elevates a new tomato system for high-throughput genome editing. *Genome Biol* **23:** 258. doi:10.1186/s13059-022-02823-7

Altschul SF, Gish W, Miller W, Myers EW, Lipman DJ. 1990. Basic local alignment search tool. *J Mol Biol* **215:** 403–410. doi:10.1016/S0022-2836(05)80360-2

Anderson JA, Song YS, Langley CH. 2008. Molecular population genetics of *Drosophila* subtelomeric DNA. *Genetics* **178:** 477–487. doi:10.1534/genetics.107.083196

Artandi SE, Depinho RA. 2009. Telomeres and telomerase in cancer. *Carcinogenesis* **31:** 9–18. doi:10.1093/carcin/bgp268

Artandi SE, Chang S, Lee SL, Alson S, Gottlieb GJ, Chin L, DePinho RA. 2000. Telomere dysfunction promotes non-reciprocal translocations and epithelial cancers in mice. *Nature* **406:** 641–645. doi:10.1038/35020592

Baumann P, Cech TR. 2001. Pot1, the putative telomere end-binding protein in fission yeast and humans. *Science* **292:** 1171–1175. doi:10.1126/science.1060036

Baur JA, Zou Y, Shay JW, Wright WE. 2001. Telomere position effect in human cells. *Science* **292:** 2075–2077. doi:10.1126/science.1062329

Beyer T, Weinert T. 2016. Ontogeny of unstable chromosomes generated by telomere error in budding yeast. *PLoS Genet* **12:** e1006345. doi:10.1371/journal.pgen.1006345

Blasco MA, Lee HW, Hande MP, Samper E, Lansdorp PM, DePinho RA, Greider CW. 1997. Telomere shortening and tumor formation by mouse cells lacking telomerase RNA. *Cell* **91:** 25–34. doi:10.1016/S0092-8674(01)80006-4

Cabanettes F, Klopp C. 2018. D-GENIES: dot plot large genomes in an interactive, efficient and simple way. *PeerJ* **6:** e4958. doi:10.7717/peerj.4958

Capper R, Britt-Compton B, Tankimanova M, Rowson J, Letsolo B, Man S, Haughton M, Baird DM. 2007. The nature of telomere fusion and a definition of the critical telomere length in human cells. *Genes Dev* **21:** 2495–2508. doi:10.1101/gad.439107

Cawthon RM. 2002. Telomere measurement by quantitative PCR. *Nucleic Acids Res* **30:** e47. doi:10.1093/nar/30.10.e47

Cesare AJ, Reddel RR. 2010. Alternative lengthening of telomeres: models, mechanisms and implications. *Nat Rev Genet* **11:** 319–330. doi:10.1038/nrg2763

Chan SW, Blackburn EH. 2003. Telomerase and ATM/Tel1p protect telomeres from nonhomologous end joining. *Mol Cell* **11:** 1379–1387. doi:10.1016/S1097-2765(03)00174-6

Chaux-Jukic F, O'Donnell S, Craig RJ, Eberhard S, Vallon O, Xu Z. 2021. Architecture and evolution of subtelomeres in the unicellular green alga *Chlamydomonas reinhardtii*. *Nucleic Acids Res* **49:** 7571–7587. doi:10.1093/nar/gkab534

Chaux-Jukic F, Agier N, Eberhard S, Xu Z. 2022. Extraction and selection of high-molecular-weight DNA for long-read sequencing from *Chlamydomonas reinhardtii*. bioRxiv doi:10.1101/2022.08.16.504088

Chen NWG, Thareau V, Ribeiro T, Magdelenat G, Ashfield T, Innes RW, Pedrosa-Harand A, Geffroy V. 2018. Common bean subtelomeres are hot spots of recombination and favor resistance gene evolution. *Front Plant Sci* **9:** 1185. doi:10.3389/fpls.2018.01185

Chin L, Artandi SE, Shen Q, Tam A, Lee SL, Gottlieb GJ, Greider CW, DePinho RA. 1999. P53 deficiency rescues the adverse effects of telomere loss and cooperates with telomere dysfunction to accelerate carcinogenesis. *Cell* **97:** 527–538. doi:10.1016/S0092-8674(00)80762-X

Corcoran LM, Thompson JK, Walliker D, Kemp DJ. 1988. Homologous recombination within subtelomeric repeat sequences generates chromosome size polymorphisms in *P. falciparum*. *Cell* **53:** 807–813. doi:10.1016/0092-8674(88)90097-9

Coutelier H, Xu Z, Morisse MC, Lhuillier-Akakpo M, Pelet S, Charvin G, Dubrana K, Teixeira MT. 2018. Adaptation to DNA damage checkpoint in senescent telomerase-negative cells promotes genome instability. *Genes Dev* **32:** 1499–1513. doi:10.1101/gad.318485.118

Craig RJ, Hasan AR, Ness RW, Keightley PD. 2021. Comparative genomics of *Chlamydomonas*. *Plant Cell* **33:** 1016–1041. doi:10.1093/plcell/koab026

Craig RJ, Gallaher SD, Shu S, Salomé P, Jenkins JW, Blaby-Haas CE, Purvine SO, O'Donnell S, Barry K, Grimwood J, et al. 2023. The *Chlamydomonas* Genome Project, version 6: reference assemblies for mating type *plus* and *minus* strains reveal extensive structural mutation in the laboratory. *Plant Cell* **35:** 644–672. doi:10.1093/plcell/koac347

Davoli T, Denchi EL, de Lange T. 2010. Persistent telomere damage induces bypass of mitosis and tetraploidy. *Cell* **141:** 81–93. doi:10.1016/j.cell.2010.01.031

Delahaye C, Nicolas J. 2021. Sequencing DNA with nanopores: troubles and biases. *PLoS One* **16:** e0257521. doi:10.1371/journal.pone.0257521

de Lange T. 2018. Shelterin-mediated telomere protection. *Annu Rev Genet* **52:** 223–247. doi:10.1146/annurev-genet-032918-021921

Eberhard S, Valuchova S, Ravat J, Fulneček J, Jolivet P, Bujaldon S, Lemaire SD, Wollman FA, Teixeira MT, Riha K, et al. 2019. Molecular characterization of *Chlamydomonas reinhardtii* telomeres and telomerase mutants. *Life Sci Alliance* **2:** e201900315. doi:10.26508/lsa.201900315

Elgin SC, Reuter G. 2013. Position-effect variegation, heterochromatin formation, and gene silencing in *Drosophila*. *Cold Spring Harb Perspect Biol* **5:** a017780. doi:10.1101/cshperspect.a017780

Fabre E, Muller H, Therizols P, Lafontaine I, Dujon B, Fairhead C. 2005. Comparative genomics in hemiascomycete yeasts: evolution of sex, silencing, and subtelomeres. *Mol Biol Evol* **22:** 856–873. doi:10.1093/molbev/msi070

Filloramo GV, Curtis BA, Blanche E, Archibald JM. 2021. Re-examination of two diatom reference genomes using long-read sequencing. *BMC Genomics* **22:** 379. doi:10.1186/s12864-021-07666-3

Flowers JM, Hazzouri KM, Pham GM, Rosas U, Bahmani T, Khraiwesh B, Nelson DR, Jijakli K, Abdrabu R, Harris EH, et al. 2015. Whole-genome resequencing reveals extensive natural variation in the model green alga *Chlamydomonas reinhardtii*. *Plant Cell* **27:** 2353–2369. doi:10.1105/tpc.15.00492

Gallaher SD, Fitz-Gibbon ST, Glaesener AG, Pellegrini M, Merchant SS. 2015. Chlamydomonas genome resource for laboratory strains reveals a mosaic of sequence variation, identifies true strain histories, and enables strain-specific studies. *Plant Cell* **27:** 2335–2352. doi:10.1105/tpc.15.00508

Gao G, Walser JC, Beaucher ML, Morciano P, Wesolowska N, Chen J, Rong YS. 2010. HipHop interacts with HOAP and HP1 to protect *Drosophila* telomeres in a sequence-independent manner. *EMBO J* **29:** 819–829. doi:10.1038/emboj.2009.394

Garsed DW, Marshall OJ, Corbin VD, Hsu A, Di Stefano L, Schröder J, Li J, Feng ZP, Kim BW, Kowarsky M, et al. 2014. The architecture and evolution of cancer neochromosomes. *Cancer Cell* **26:** 653–667. doi:10.1016/j.ccell.2014.09.010

Gottschling DE, Aparicio OM, Billington BL, Zakian VA. 1990. Position effect at *S. cerevisiae* telomeres: reversible repression of Pol II transcription. *Cell* **63:** 751–762. doi:10.1016/0092-8674(90)90141-Z

Hackett JA, Greider CW. 2003. End resection initiates genomic instability in the absence of telomerase. *Mol Cell Biol* **23:** 8450–8461. doi:10.1128/MCB.23.23.8450-8461.2003

Hackett JA, Feldser DM, Greider CW. 2001. Telomere dysfunction increases mutation rate and genomic instability. *Cell* **106:** 275–286. doi:10.1016/S0092-8674(01)00457-3

Hails T, Jobling M, Day A. 1993. Large arrays of tandemly repeated DNA sequences in the green alga *Chlamydomonas reinhardtii*. *Chromosoma* **102:** 500–507. doi:10.1007/BF00357106

Harris EH. 2009. *The Chlamydomonas sourcebook*. Elsevier/Academic Press, Oxford.

Hastings PJ, Ira G, Lupski JR. 2009. A microhomology-mediated break-induced replication model for the origin of human copy number variation. *PLoS Genet* **5:** e1000327. doi:10.1371/journal.pgen.1000327

Heacock M, Spangler E, Riha K, Puizina J, Shippen DE. 2004. Molecular analysis of telomere fusions in *Arabidopsis*: multiple pathways for chromosome end-joining. *EMBO J* **23:** 2304–2313. doi:10.1038/sj.emboj.7600236

Henninger E, Teixeira MT. 2020. Telomere-driven mutational processes in yeast. *Curr Opin Genet Dev* **60:** 99–106. doi:10.1016/j.gde.2020.02.018

Henson JD, Lau LM, Koch S, La Rotta N M, Dagg RA, Reddel RR. 2017. The C-circle assay for alternative-lengthening-of-telomeres activity. *Methods* **114:** 74–84. doi:10.1016/j.ymeth.2016.08.016

Ho SS, Urban AE, Mills RE. 2020. Structural variation in the sequencing era. *Nat Rev Genet* **21:** 171–189. doi:10.1038/s41576-019-0180-9

Jain D, Cooper JP. 2010. Telomeric strategies: means to an end. *Annu Rev Genet* **44:** 243–269. doi:10.1146/annurev-genet-102108-134841

Jain D, Hebden AK, Nakamura TM, Miller KM, Cooper JP. 2010. HAATI survivors replace canonical telomeres with blocks of generic heterochromatin. *Nature* **467:** 223–227. doi:10.1038/nature09374

Jones K. 1998. Robertsonian fusion and centric fission in karyotype evolution of higher plants. *Bot Rev* **64:** 273–289. doi:10.1007/BF02856567

Jones RE, Oh S, Grimstead JW, Zimbric J, Roger L, Heppel NH, Ashelford KE, Liddiard K, Hendrickson EA, Baird DM. 2014. Escape from telomere-driven crisis is DNA ligase III dependent. *Cell Rep* **8:** 1063–1076. doi:10.1016/j.celrep.2014.07.007

Kim JM, Vanguri S, Boeke JD, Gabriel A, Voytas DF. 1998. Transposable elements and genome organization: a comprehensive survey of

retrotransposons revealed by the complete *Saccharomyces cerevisiae* genome sequence. *Genome Res* **8:** 464–478. doi:10.1101/gr.8.5.464
Kim C, Kim J, Kim S, Cook DE, Evans KS, Andersen EC, Lee J. 2019. Long-read sequencing reveals intra-species tolerance of substantial structural variations and new subtelomere formation in *C. elegans*. *Genome Res* **29:** 1023–1035. doi:10.1101/gr.246082.118
Kim E, Kim J, Kim C, Lee J. 2021. Long-read sequencing and de novo genome assemblies reveal complex chromosome end structures caused by telomere dysfunction at the single nucleotide level. *Nucleic Acids Res* **49:** 3338–3353. doi:10.1093/nar/gkab141
Kockler ZW, Comeron JM, Malkova A. 2021. A unified alternative telomere-lengthening pathway in yeast survivor cells. *Mol Cell* **81:** 1816–1829.e5. doi:10.1016/j.molcel.2021.02.004
Koering CE, Pollice A, Zibella MP, Bauwens S, Puisieux A, Brunori M, Brun C, Martins L, Sabatier L, Pulitzer JF, et al. 2002. Human telomeric position effect is determined by chromosomal context and telomeric chromatin integrity. *EMBO Rep* **3:** 1055–1061. doi:10.1093/embo-reports/kvf215
Kolmogorov M, Yuan J, Lin Y, Pevzner PA. 2019. Assembly of long, error-prone reads using repeat graphs. *Nat Biotechnol* **37:** 540–546. doi:10.1038/s41587-019-0072-8
Koren S, Walenz BP, Berlin K, Miller JR, Bergman NH, Phillippy AM. 2017. Canu: scalable and accurate long-read assembly via adaptive *k*-mer weighting and repeat separation. *Genome Res* **27:** 722–736. doi:10.1101/gr.215087.116
Krzywinski M, Schein J, Birol I, Connors J, Gascoyne R, Horsman D, Jones SJ, Marra MA. 2009. Circos: an information aesthetic for comparative genomics. *Genome Res* **19:** 1639–1645. doi:10.1101/gr.092759.109
Kuo HF, Olsen KM, Richards EJ. 2006. Natural variation in a subtelomeric region of *Arabidopsis*: implications for the genomic dynamics of a chromosome end. *Genetics* **173:** 401–417. doi:10.1534/genetics.105.055202
Larkin MA, Blackshields G, Brown NP, Chenna R, McGettigan PA, McWilliam H, Valentin F, Wallace IM, Wilm A, Lopez R, et al. 2007. Clustal W and Clustal X version 2.0. *Bioinformatics* **23:** 2947–2948. doi:10.1093/bioinformatics/btm404
Lee HW, Blasco MA, Gottlieb GJ, Horner JW 2nd, Greider CW, DePinho RA. 1998. Essential role of mouse telomerase in highly proliferative organs. *Nature* **392:** 569–574. doi:10.1038/33345
Li H. 2018. Minimap2: pairwise alignment for nucleotide sequences. *Bioinformatics* **34:** 3094–3100. doi:10.1093/bioinformatics/bty191
Li H, Handsaker B, Wysoker A, Fennell T, Ruan J, Homer N, Marth G, Abecasis G, Durbin R, 1000 Genome Project Data Processing Subgroup. 2009. The Sequence Alignment/Map format and SAMtools. *Bioinformatics* **25:** 2078–2079. doi:10.1093/bioinformatics/btp352
Li Y, Schwab C, Ryan S, Papaemmanuil E, Robinson HM, Jacobs P, Moorman AV, Dyer S, Borrow J, Griffiths M, et al. 2014. Constitutional and somatic rearrangement of chromosome 21 in acute lymphoblastic leukaemia. *Nature* **508:** 98–102. doi:10.1038/nature13115
Li X, Zhang R, Patena W, Gang SS, Blum SR, Ivanova N, Yue R, Robertson JM, Lefebvre PA, Fitz-Gibbon ST, et al. 2016. An indexed, mapped mutant library enables reverse genetics studies of biological processes in *Chlamydomonas reinhardtii*. *Plant Cell* **28:** 367–387. doi:10.1105/tpc.15.00465
Linardopoulou EV, Williams EM, Fan Y, Friedman C, Young JM, Trask BJ. 2005. Human subtelomeres are hot spots of interchromosomal recombination and segmental duplication. *Nature* **437:** 94–100. doi:10.1038/nature04029
Liu Q, Fang L, Yu G, Wang D, Xiao CL, Wang K. 2019. Detection of DNA base modifications by deep recurrent neural network on Oxford Nanopore sequencing data. *Nat Commun* **10:** 2449. doi:10.1038/s41467-019-10168-2
Liu H, Wu S, Li A, Ruan J. 2021. SMARTdenovo: a *de novo* assembler using long noisy reads. *GigaByte* **2021:** gigabyte15. doi:10.46471/gigabyte.15
López-Cortegano E, Craig RJ, Chebib J, Balogun EJ, Keightley PD. 2023. Rates and spectra of de novo structural mutations in *Chlamydomonas reinhardtii*. *Genome Res* **33:** 45–60. doi:10.1101/gr.276957.122
Louis EJ. 1995. The chromosome ends of *Saccharomyces cerevisiae*. *Yeast* **11:** 1553–1573. doi:10.1002/yea.320111604
Louis EJ, Haber JE. 1990. Mitotic recombination among subtelomeric Y′ repeats in *Saccharomyces cerevisiae*. *Genetics* **124:** 547–559. doi:10.1093/genetics/124.3.547
Lowden MR, Meier B, Lee TW, Hall J, Ahmed S. 2008. End joining at *Caenorhabditis elegans* telomeres. *Genetics* **180:** 741–754. doi:10.1534/genetics.108.089920
Lundblad V, Blackburn EH. 1993. An alternative pathway for yeast telomere maintenance rescues *est1*$^-$ senescence. *Cell* **73:** 347–360. doi:10.1016/0092-8674(93)90234-H
Maciejowski J, de Lange T. 2017. Telomeres in cancer: tumour suppression and genome instability. *Nat Rev Mol Cell Biol* **18:** 175–186. doi:10.1038/nrm.2016.171
Maciejowski J, Li Y, Bosco N, Campbell PJ, de Lange T. 2015. Chromothripsis and kataegis induced by telomere crisis. *Cell* **163:** 1641–1654. doi:10.1016/j.cell.2015.11.054
Maestroni L, Audry J, Matmati S, Arcangioli B, Géli V, Coulon S. 2017. Eroded telomeres are rearranged in quiescent fission yeast cells through duplications of subtelomeric sequences. *Nat Commun* **8:** 1684. doi:10.1038/s41467-017-01894-6
Matsuda A, Chikashige Y, Ding DQ, Ohtsuki C, Mori C, Asakawa H, Kimura H, Haraguchi T, Hiraoka Y. 2015. Highly condensed chromatins are formed adjacent to subtelomeric and decondensed silent chromatin in fission yeast. *Nat Commun* **6:** 7753. doi:10.1038/ncomms8753
McClintock B. 1941. The stability of broken ends of chromosomes in *Zea mays*. *Genetics* **26:** 234–282. doi:10.1093/genetics/26.2.234
McEachern MJ, Iyer S, Fulton TB, Blackburn EH. 2000. Telomere fusions caused by mutating the terminal region of telomeric DNA. *Proc Natl Acad Sci USA* **97:** 11409–11414. doi:10.1073/pnas.210388397
Mieczkowski PA, Mieczkowska JO, Dominska M, Petes TD. 2003. Genetic regulation of telomere-telomere fusions in the yeast *Saccharomyces cerevisiae*. *Proc Natl Acad Sci USA* **100:** 10854–10859. doi:10.1073/pnas.1934561100
Milne I, Stephen G, Bayer M, Cock PJ, Pritchard L, Cardle L, Shaw PD, Marshall D. 2013. Using tablet for visual exploration of second-generation sequencing data. *Brief Bioinform* **14:** 193–202. doi:10.1093/bib/bbs012
Naito T, Matsuura A, Ishikawa F. 1998. Circular chromosome formation in a fission yeast mutant defective in two ATM homologues. *Nat Genet* **20:** 203–206. doi:10.1038/2517
Nakamura TM, Cooper JP, Cech TR. 1998. Two modes of survival of fission yeast without telomerase. *Science* **282:** 493–496. doi:10.1126/science.282.5388.493
O'Donnell S, Fischer G. 2020. MUM&co: accurate detection of all SV types through whole-genome alignment. *Bioinformatics* **36:** 3242–3243. doi:10.1093/bioinformatics/btaa115
O'Donnell S, Chaux F, Fischer G. 2020. Highly contiguous nanopore genome assembly of *Chlamydomonas reinhardtii* CC-1690. *Microbiol Resour Announc* **9:** e00726-20. doi:10.1128/MRA.00726-20
Otto TD, Böhme U, Sanders M, Reid A, Bruske EI, Duffy CW, Bull PC, Pearson RD, Abdi A, Dimonte S, et al. 2018. Long read assemblies of geographically dispersed plasmodium falciparum isolates reveal highly structured subtelomeres. *Wellcome Open Res* **3:** 52. doi:10.12688/wellcomeopenres.14571.1
Pardo B, Marcand S. 2005. Rap1 prevents telomere fusions by nonhomologous end joining. *EMBO J* **24:** 3117–3127. doi:10.1038/sj.emboj.7600778
Payen C, Koszul R, Dujon B, Fischer G. 2008. Segmental duplications arise from Pol32-dependent repair of broken forks through two alternative replication-based mechanisms. *PLoS Genet* **4:** e1000175. doi:10.1371/journal.pgen.1000175
Payne ZL, Penny GM, Turner TN, Dutcher SK. 2023. A gap-free genome assembly of *Chlamydomonas reinhardtii* and detection of translocations induced by CRISPR-mediated mutagenesis. *Plant Commun* **4:** 100493. doi:10.1016/j.xplc.2022.100493
Pedram M, Sprung CN, Gao Q, Lo AW, Reynolds GE, Murnane JP. 2006. Telomere position effect and silencing of transgenes near telomeres in the mouse. *Mol Cell Biol* **26:** 1865–1878. doi:10.1128/MCB.26.5.1865-1878.2006
Pobiega S, Marcand S. 2010. Dicentric breakage at telomere fusions. *Genes Dev* **24:** 720–733. doi:10.1101/gad.571510
Quinlan AR, Hall IM. 2010. BEDTools: a flexible suite of utilities for comparing genomic features. *Bioinformatics* **26:** 841–842. doi:10.1093/bioinformatics/btq033
R Core Team. 2021. *R: a language and environment for statistical computing*. R Foundation for Statistical Computing, Vienna. https://www.R-project.org/.
Richard MM, Chen NW, Thareau V, Pflieger S, Blanchet S, Pedrosa-Harand A, Iwata A, Chavarro C, Jackson SA, Geffroy V. 2013. The subtelomeric *khipu* satellite repeat from *Phaseolus vulgaris*: lessons learned from the genome analysis of the Andean genotype G19833. *Front Plant Sci* **4:** 109. doi:10.3389/fpls.2013.00109
Robertson WRB. 1916. Chromosome studies. I. Taxonomic relationships shown in the chromosomes of Tettigidae and Acrididae: V-shaped chromosomes and their significance in Acrididae, Locustidae, and Gryllidae: chromosomes and variation. *J Morphol* **27:** 179–331. doi:10.1002/jmor.1050270202
Robinson JT, Thorvaldsdóttir H, Wenger AM, Zehir A, Mesirov JP. 2017. Variant review with the integrative genomics viewer. *Cancer Res* **77:** e31–e34. doi:10.1158/0008-5472.CAN-17-0337
Rudd MK, Friedman C, Parghi SS, Linardopoulou EV, Hsu L, Trask BJ. 2007. Elevated rates of sister chromatid exchange at chromosome ends. *PLoS Genet* **3:** e32. doi:10.1371/journal.pgen.0030032

Sabatier L, Ricoul M, Pottier G, Murnane JP. 2005. The loss of a single telomere can result in instability of multiple chromosomes in a human tumor cell line. *Mol Cancer Res* **3:** 139–150. doi:10.1158/1541-7786.MCR-04-0194

Sfeir A, Symington LS. 2015. Microhomology-mediated end joining: a back-up survival mechanism or dedicated pathway? *Trends Biochem Sci* **40:** 701–714. doi:10.1016/j.tibs.2015.08.006

Sholes SL, Karimian K, Gershman A, Kelly TJ, Timp W, Greider CW. 2021. Chromosome-specific telomere lengths and the minimal functional telomere revealed by nanopore sequencing. *Genome Res* **32:** 616–628. doi:10.1101/gr.275868.121

Simpson JT, Workman RE, Zuzarte PC, David M, Dursi LJ, Timp W. 2017. Detecting DNA cytosine methylation using nanopore sequencing. *Nat Methods* **14:** 407–410. doi:10.1038/nmeth.4184

Stortchevoi A, Kamelamela N, Levine SS. 2020. SPRI beads-based size selection in the range of 2-10kb. *J Biomol Tech* **31:** 7–10. doi:10.7171/jbt.20-3101-002

Strenkert D, Schmollinger S, Schroda M. 2013. Heat shock factor 1 counteracts epigenetic silencing of nuclear transgenes in *Chlamydomonas reinhardtii*. *Nucleic Acids Res* **41:** 5273–5289. doi:10.1093/nar/gkt224

Takikawa M, Tarumoto Y, Ishikawa F. 2017. Fission yeast Stn1 is crucial for semi-conservative replication at telomeres and subtelomeres. *Nucleic Acids Res* **45:** 1255–1269. doi:10.1093/nar/gkw1176

Teng SC, Zakian VA. 1999. Telomere-telomere recombination is an efficient bypass pathway for telomere maintenance in *Saccharomyces cerevisiae*. *Mol Cell Biol* **19:** 8083–8093. doi:10.1128/MCB.19.12.8083

Umbreit NT, Zhang CZ, Lynch LD, Blaine LJ, Cheng AM, Tourdot R, Sun L, Almubarak HF, Judge K, Mitchell TJ, et al. 2020. Mechanisms generating cancer genome complexity from a single cell division error. *Science* **368:** eaba0712. doi:10.1126/science.aba0712

Vaquero-Sedas MI, Gámez-Arjona FM, Vega-Palas MA. 2011. *Arabidopsis thaliana* telomeres exhibit euchromatic features. *Nucleic Acids Res* **39:** 2007–2017. doi:10.1093/nar/gkq1119

Vaser R, Sović I, Nagarajan N, Šikić M. 2017. Fast and accurate de novo genome assembly from long uncorrected reads. *Genome Res* **27:** 737–746. doi:10.1101/gr.214270.116

Vrbsky J, Akimcheva S, Watson JM, Turner TL, Daxinger L, Vyskot B, Aufsatz W, Riha K. 2010. siRNA-mediated methylation of *Arabidopsis* telomeres. *PLoS Genet* **6:** e1000986. doi:10.1371/journal.pgen.1000986

Wick RR, Schultz MB, Zobel J, Holt KE. 2015. Bandage: interactive visualization of de novo genome assemblies. *Bioinformatics* **31:** 3350–3352. doi:10.1093/bioinformatics/btv383

Wu ZJ, Liu JC, Man X, Gu X, Li TY, Cai C, He MH, Shao Y, Lu N, Xue X, et al. 2020. Cdc13 is predominant over Stn1 and Ten1 in preventing chromosome end fusions. *eLife* **9:** e53144. doi:10.7554/eLife.53144

Young E, Abid HZ, Kwok PY, Riethman H, Xiao M. 2020. Comprehensive analysis of human subtelomeres by whole genome mapping. *PLoS Genet* **16:** e1008347. doi:10.1371/journal.pgen.1008347

Yue JX, Li J, Aigrain L, Hallin J, Persson K, Oliver K, Bergström A, Coupland P, Warringer J, Lagomarsino MC, et al. 2017. Contrasting evolutionary genome dynamics between domesticated and wild yeasts. *Nat Genet* **49:** 913–924. doi:10.1038/ng.3847

Zellinger B, Akimcheva S, Puizina J, Schirato M, Riha K. 2007. Ku suppresses formation of telomeric circles and alternative telomere lengthening in *Arabidopsis*. *Mol Cell* **27:** 163–169. doi:10.1016/j.molcel.2007.05.025

Received April 27, 2023; accepted in revised form August 9, 2023.

Telomerase-independent survival leads to a mosaic of complex subtelomere rearrangements in *Chlamydomonas reinhardtii*

Frédéric Chaux, Nicolas Agier, Clotilde Garrido, et al.

Genome Res. published online August 14, 2023
Access the most recent version at doi:10.1101/gr.278043.123